NASA TECHNICAL NOTE

NASA TN D-2390

NASA TN D-2390

NUMERICAL CALCULATION OF SUPERSONIC FLOWS OF A PERFECT GAS OVER BODIES OF REVOLUTION AT SMALL ANGLES OF YAW

by John V. Rakich

Ames Research Center
Moffett Field, Calif.

NATIONAL AERONAUTICS AND SPACE ADMINISTRATION • WASHINGTON, D. C. • JULY 1964

NUMERICAL CALCULATION OF SUPERSONIC FLOWS OF A PERFECT GAS OVER BODIES OF REVOLUTION AT SMALL ANGLES OF YAW

By John V. Rakich

Ames Research Center
Moffett Field, Calif.

NATIONAL AERONAUTICS AND SPACE ADMINISTRATION

For sale by the Office of Technical Services, Department of Commerce,
Washington, D.C. 20230 -- Price $1.50

NUMERICAL CALCULATION OF SUPERSONIC FLOWS OF A PERFECT GAS OVER BODIES OF REVOLUTION AT SMALL ANGLES OF YAW

By John V. Rakich

Ames Research Center
Moffett Field, Calif.

SUMMARY

A linearized characteristics method is used to obtain the first-order effects of yaw in the supersonic portion of the flow over bodies of revolution. The first-order perturbation equations are derived in terms of pressure and flow-deflection angles as dependent variables and are incorporated into an existing method of characteristics computer program for axisymmetric flow. Some example flows obtained from the resulting program are presented for the purpose of establishing the accuracy and applicability of the method.

The method yields results which are in agreement with Kopal's exact solutions for cone flow, and surface pressures for blunt-nosed cones tend to the pointed cone values at a large distance from the nose. The first-order perturbation field for a sphere-cone is compared with published results obtained by basically the same method; there is a general agreement of the results, but some differences are noted. For an ogive of fineness ratio 3, comparison with experiment and shock-expansion theories indicates applicability for yaw angles up to about 5°. In the case of spherically blunted 15° and 30° cones, the present theory agrees well with experiment for yaw angles up to 2° and 5°, respectively. Estimates based on pointed cone theories indicate the range of angles to which the present linear approximation can be applied.

INTRODUCTION

The subsonic region near the stagnation point of a blunt body has only recently, and with the help of modern computers, been accurately determined (see, e.g., refs. 1 and 2). These "blunt body" solutions typically extend only slightly into the region of supersonic flow and it has been necessary to use the method of characteristics in order to continue the solutions into the supersonic region. This matching of the two methods of solution has been achieved for unyawed bodies of revolution (ref. 3). In the present paper, the method of characteristics is used to continue the blunt body solution into the supersonic region for the case of a yawed body of revolution. However, to avoid the complexity of a three-dimensional characteristics approach, well-established perturbation techniques are used (refs. 4 to 13). The procedure of coupling the method of characteristics with the perturbation technique is

called a linearized characteristics method (ref. 8). Its theoretical basis is adequately covered in the referenced works and will not be repeated herein. However, the present equations and procedures differ in some details from those of the references. Therefore the equations used in the computer program will be derived and some aspects of the program described. Results for a few selected bodies will be presented and compared with experiment and with the results of other theories.

Subsequent to the initiation of the present study, reference 14 presented results of calculations of the supersonic flow over a spherically blunted cone at small yaw. These results were obtained by basically the same method used in the present study (i.e., linearized characteristics method). Some of the results of reference 14 are reproduced in the present paper for comparison, and some differences with present results and techniques are discussed.

SYMBOLS

a	speed of sound
c_p	specific heat at constant pressure
c_v	specific heat at constant volume
C_N	normal-force coefficient
C_p	pressure coefficient
d	body diameter
f	fineness ratio, $\frac{L}{d}$
h	enthalpy
K	constant in body boundary condition (eq. (26))
K_τ, K_α	hypersonic similarity parameters
L	body length
M	Mach number
p	pressure

r	radial coordinate, cylindrical coordinate system
R	radial distance to shock wave
R_b	nose radius for blunt-nosed body
S	entropy
u	velocity component in x direction
v	velocity component in r direction
V	scalar magnitude of velocity vector ($\vec{V} = V\vec{s}$)
$\vec{V}$	velocity vector
w	velocity component in circumferential direction (crossflow velocity)
$\overline{x}$	distance to center of pressure
x,r,z	cylindrical coordinates
x,y,z	rectangular coordinates
s,n,t	streamline coordinates (see fig. 1)
$\vec{i},\vec{j},\vec{k}$	unit vectors, rectangular coordinates
$\vec{e}_x,\vec{e}_r,\vec{e}_\Phi$	unit vectors, cylindrical coordinates
$\vec{s},\vec{n},\vec{t}$	unit vectors, streamline coordinates
$\vec{e}_s,\vec{e}_n,\vec{e}_t$	shock-oriented unit vectors
α	angle of yaw, radians
β	$\sqrt{M^2 - 1}$
γ	specific-heat ratio
η	left-running characteristic coordinate
θ	flow angle measured from x axis in meridional plane, $\tan^{-1}\frac{v}{u}$ (fig. 1)
ξ	right-running characteristic coordinate
ρ	density
σ	shock-wave angle measured from x axis

φ crossflow angle, $\sin^{-1}\frac{w}{V}$

Φ azimuthal coordinate, cylindrical coordinate system

Subscripts

o zero-order variable from solution of axisymmetric, nonyaw flow

1 first-order perturbation variable, implies a derivative with respect to α which is a function of x and r only, as defined by equations (3) and (45)

α first-order perturbation variable, implies a derivative with respect to α which is a function of x, r, and Φ, as defined by equations (4)

∞ free-stream conditions

B conditions on the body

m coordinates fixed with respect to the meridional plane (fig. 1)

S conditions immediately behind the shock wave

Superscripts

' coordinates fixed with respect to the body axis

" coordinates fixed with respect to the shock axis

DEVELOPMENT OF THE EQUATIONS AND BOUNDARY CONDITIONS

Calculation of the flow over a specified body by the method of characteristics usually requires that initial conditions be specified along some curve between the body and the shock wave. For unyawed bodies of revolution, the starting (initial) data are obtained from cone flow solutions for pointed bodies and from blunt-body solutions for blunt-nosed bodies. The present problem of yawed bodies of revolution therefore requires solutions for yawed cones and yawed blunt bodies to provide starting data. While solutions for yawed cones are available (ref. 4), none are currently available for the general blunt body. However, for a spherical body, the axisymmetric solution is independent of the yaw angle and therefore provides starting data for yawed bodies with spherical tips. It is only necessary that any deviations from the spherical shape should occur in the supersonic region of flow (or, more precisely, downstream of the limiting characteristic between the sonic line and the body).

In the present development of the equations, the initial data are assumed given by the appropriate cone or sphere solution and, also, the entire flow field for the unyawed body is assumed known from previous calculation. The problem then is to develop the equations and boundary conditions for the perturbation flow field due to yawing the body by a small angle. The analysis is confined to the supersonic portion of the flow field and will make use of the method of characteristics. The method will not be developed from its basic elements, since this was done previously (refs. 8, 15, or 16, e.g.). In reference 8 it is shown that the characteristics of the perturbation field are identical with those of the axisymmetric flow. The first step of the analysis will be to obtain the first-order perturbation equations which describe the flow along these characteristic directions; these are the compatibility equations of characteristics theory.

Equations

The required compatibility equations can be derived in a variety of forms depending on the choice of dependent variables. One of the simpler forms is obtained if pressure and flow angles are chosen as dependent variables (see, e.g., ref. 16). This approach is followed herein, and the analysis begins with the equations of motion expressed in intrinsic or streamline coordinates. However, since the equations in reference 16 are valid only for two-dimensional or axisymmetric flows, it will be necessary first to obtain them in a more general form. This is done in appendix A. There it is shown that for flows which deviate only slightly from axisymmetric flow, the following equations apply

$$\frac{\beta^2}{\gamma p M^2}\frac{\partial p}{\partial s} + \frac{\partial \theta}{\partial n} + \frac{\partial \varphi}{\partial t} + \frac{\sin\theta}{r} = 0 \tag{1a}$$

$$\frac{1}{\gamma p M^2}\frac{\partial p}{\partial n} + \frac{\partial \theta}{\partial s} = 0 \tag{1b}$$

$$\frac{1}{\gamma p M^2}\frac{\partial p}{\partial t} + \frac{\partial \varphi}{\partial s} + \frac{\varphi \sin\theta}{r} = 0 \tag{1c}$$

The intrinsic coordinates (s,n,t) used in these equations are illustrated in figure 1 in terms of a unit vector $\vec{s}$, parallel to the velocity vector $\vec{V}$, and unit vectors $\vec{n}$ and $\vec{t}$, normal to $\vec{V}$; the normal $\vec{n}$ lies in the meridional plane, Φ = constant. This orthogonal set may be described in terms of two rotations of a reference system of axes (x_m, r_m, z_m) initially fixed with respect to the meridional plane. The initial system is rotated by angle θ about the z_m axis, and the resultant system is rotated by angle φ about the n axis to produce the desired s,n,t system. The angle θ is called the flow angle and φ the crossflow angle. These angles and the pressure are the dependent variables in equations (1).

Expansions for the dependent variables.- The usual procedure for obtaining the perturbation equations is to expand all dependent variables in the

following type of series

$$p(x,r,\Phi;\alpha) = p_o(x,r) + \alpha\left[\sum_l p_l(x,r)\cos\, l\Phi + \sum_m p_m(x,r)\sin\, m\Phi\right] \qquad (2)$$

where x, r, Φ are cylindrical coordinates (fig. 1), and p_o is obtained from the solution of the nonyaw problem. For the first-order yaw problem, however, it is shown in references 4 and 8 that to be consistent with the boundary conditions, it is necessary to retain only the first term of the sine series for crossflow angle (or crossflow velocity) and the first term of the cosine series for all other variables. Thus, in practice, the expressions used are

$$\left.\begin{aligned} p(x,r,\Phi;\alpha) &= p_o(x,r) + \alpha p_1(x,r)\cos\,\Phi \\ \theta(x,r,\Phi;\alpha) &= \theta_o(x,r) + \alpha\theta_1(x,r)\cos\,\Phi \\ \varphi(x,r,\Phi;\alpha) &= \alpha\varphi_1(x,r)\sin\,\Phi \\ &\text{etc.} \end{aligned}\right\} \qquad (3)$$

It will be convenient at times to use perturbation quantities which contain the Φ dependence. These will be denoted by an α subscript and defined as follows

$$\left.\begin{aligned} p_\alpha(x,r,\Phi) &= p_1(x,r)\cos\,\Phi \\ \theta_\alpha(x,r,\Phi) &= \theta_1(x,r)\cos\,\Phi \\ \varphi_\alpha(x,r,\Phi) &= \varphi_1(x,r)\sin\,\Phi \\ &\text{etc.} \end{aligned}\right\} \qquad (4)$$

These perturbation quantities may also be identified as derivatives with respect to yaw angle (e.g., $p_\alpha = (\partial p/\partial\alpha)_{\alpha=0}$). However, for brevity, the notation indicated in equations (3) and (4) will be used in the development of the method and in the results.

Expansions for the derivatives.- In addition to the substitutions given above for the dependent variables, expansions must also be developed for the independent variables s,n,t which appear in the derivatives in equations (1). Specifically, a transformation is needed which resolves the derivatives $\partial/\partial s$, $\partial/\partial n$, $\partial/\partial t$ into components along the intrinsic coordinates s_o,n_o,t_o of the zero yaw flow field. To this end the set of unit vectors $\vec{s},\vec{n},\vec{t}$ in figure 1 is written in terms of the corresponding set for zero yaw $\vec{s}_o,\vec{n}_o,\vec{t}_o$, plus two small rotations. This is illustrated in figure 2 which shows the x_m,r_m,z_m coordinate system of figure 1 in a different view. The first rotation is about $\vec{t}_o$ by angle $\alpha\theta_\alpha$, and the second about $\vec{n}_o$ by angle $\alpha\varphi_\alpha$. It is easily verified by inspection of figure 2 that the following vector relationships hold to the order of this analysis.

$$\vec{s} = \vec{s}_o + \alpha\theta_\alpha \vec{n}_o + \alpha\varphi_\alpha \vec{t}_o \tag{5a}$$

$$\vec{n} = \vec{n}_o - \alpha\theta_\alpha \vec{s}_o \tag{5b}$$

$$\vec{t} = \vec{t}_o - \alpha\varphi_\alpha \vec{s}_o \tag{5c}$$

Thus, to first order in α, the gradients along the $\vec{s}$, $\vec{n}$, and $\vec{t}$ directions are

$$\frac{\partial}{\partial s} = \frac{\partial}{\partial s_o} + \alpha\left(\theta_\alpha \frac{\partial}{\partial n_o} + \varphi_\alpha \frac{\partial}{\partial t_o}\right) \tag{6a}$$

$$\frac{\partial}{\partial n} = \frac{\partial}{\partial n_o} - \alpha\theta_\alpha \frac{\partial}{\partial s_o} \tag{6b}$$

$$\frac{\partial}{\partial t} = \frac{\partial}{\partial t_o} - \alpha\varphi_\alpha \frac{\partial}{\partial s_o} \tag{6c}$$

First-order perturbation equations.- All necessary elements are now available so that the corresponding first-order equations can be deduced from equations (1). However, in order to reduce the number of perturbation quantities, it will be convenient to express the Mach number perturbations in terms of pressure and density perturbations as follows.

$$M = \frac{V}{a} = \frac{V_o}{a_o} + \alpha \frac{V_o}{a_o}\left(\frac{V_\alpha}{V_o} - \frac{a_\alpha}{a_o}\right) \tag{7}$$

The sound-speed perturbation, a_α, can, in turn, be eliminated by use of the energy equation in its integrated form

$$a^2 + \left(\frac{\gamma - 1}{2}\right) V^2 = a_t^2 = \text{constant} \tag{8}$$

which yields

$$a^2 = a_o^2 - \alpha(\gamma - 1)V_o V_\alpha = a_o^2 + 2\alpha a_o a_\alpha$$

and

$$a_\alpha = -\left(\frac{\gamma - 1}{2}\right) M_o V_\alpha \tag{9}$$

On the other hand, the sound speed may be eliminated in favor of pressure and density by the relation

$$a^2 = \gamma \frac{p}{\rho} \tag{10}$$

Applying the linearizing procedure and combining with equation (9) gives the following expression for the velocity perturbation in terms of pressure and density perturbations

$$\frac{V_\alpha}{V_o} = - \frac{1}{(\gamma - 1)M_o^2} \left(\frac{p_\alpha}{p_o} - \frac{\rho_\alpha}{\rho_o} \right) \tag{11}$$

which, with equations (9) and (7), gives the desired expression

$$M_\alpha = - \frac{M_o}{2} \left(\frac{p_\alpha}{p_o} - \frac{\rho_\alpha}{\rho_o} \right) \left[1 + \frac{2}{(\gamma - 1)M_o^2} \right] \tag{12}$$

Equations (3), (4), (6), and (12) can be used to obtain the following first-order perturbation equations from equations (1):

$$\frac{\partial \theta_1}{\partial n_o} + \frac{\beta_o^2}{\gamma p_o M_o^2} \frac{\partial p_1}{\partial s_o} = - \frac{1}{r}(\varphi_1 + \theta_1 \cos \theta_o) + \left\{ \frac{p_1}{p_o} + \left(\frac{p_1}{p_o} - \frac{\rho_1}{\rho_o} \right) \left[\frac{1 + \frac{2}{(\gamma - 1)M_o^2}}{\beta_o^2} \right] \right\} \frac{\beta_o^2}{\gamma p_o M_o^2} \frac{\partial p_o}{\partial s_o} - \theta_1 \left(\frac{\beta_o^2}{\gamma p_o M_o^2} \frac{\partial p_o}{\partial n_o} - \frac{\partial \theta_o}{\partial s_o} \right) \tag{13a}$$

$$\frac{\partial \theta_1}{\partial s_o} + \frac{1}{\gamma p_o M_o^2} \frac{\partial p_1}{\partial n_o} = \left\{ \frac{p_1}{p_o} - \left(\frac{p_1}{p_o} - \frac{\rho_1}{\rho_o} \right) \left[1 + \frac{2}{(\gamma - 1)M_o^2} \right] \right\} \frac{1}{\gamma p_o M_o^2} \frac{\partial p_o}{\partial n_o} + \theta_1 \left(\frac{1}{\gamma p_o M_o^2} \frac{\partial p_o}{\partial s_o} - \frac{\partial \theta_o}{\partial n_o} \right) \tag{13b}$$

$$\frac{\partial \varphi_1}{\partial s_o} = \varphi_1 \left(\frac{1}{\gamma p_o M_o^2} \frac{\partial p_o}{\partial s_o} - \frac{\sin \theta_o}{r} \right) + \frac{p_1}{r \gamma p_o M_o^2} \tag{13c}$$

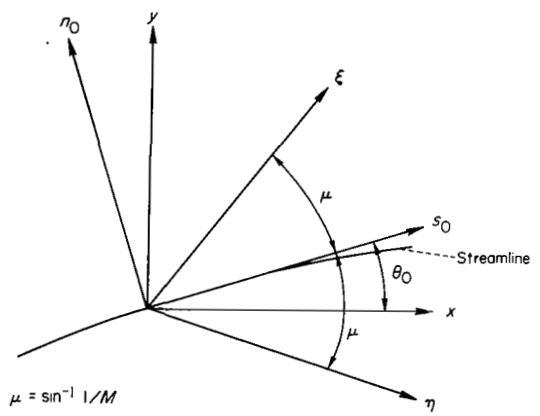

Sketch (a)

It is noted that equations (13) are independent of the azimuthal angle Φ, and the problem is reduced to one involving only two space variables. For the solution of this problem by the method of characteristics it is necessary to project the first two of equations (13) into the characteristic directions ξ and η (sketch (a)); equation (13c) is already in the desired form since it contains the derivative of φ_1 in the third characteristic direction, that is, along the streamline s_o. To obtain these equations,

the approach given in references 17 and 18 is used. Thus, application of the following transformation from s_o, n_o to ξ, η coordinates

$$\left.\begin{aligned} \frac{\partial}{\partial s_o} &= \frac{M_o}{2\beta_o}\left(\frac{\partial}{\partial \eta} + \frac{\partial}{\partial \xi}\right) \\ \frac{\partial}{\partial n_o} &= \frac{M_o}{2}\left(\frac{\partial}{\partial \eta} - \frac{\partial}{\partial \xi}\right) \end{aligned}\right\} \tag{14}$$

results, after some manipulation, in equations for p_1 and θ_1 which involve derivatives in one direction only (i.e., the compatibility equations of characteristic theory). These are the following equations upon which the present numerical computations are based:

$$A\frac{\partial p_1}{\partial \eta} + \frac{\partial \theta_1}{\partial \eta} = F_1 - G \tag{15a}$$

$$A\frac{\partial p_1}{\partial \xi} - \frac{\partial \theta_1}{\partial \xi} = F_2 - G \tag{15b}$$

where the coefficients are

$$F_1 = \frac{A_o}{M_o}\left[(\beta_o B + \theta_1)\frac{\partial p_o}{\partial s_o} + (C - \beta_o \theta_1)\frac{\partial p_o}{\partial n_o}\right] + \frac{\theta_1}{M_o}\left(\frac{\partial \theta_o}{\partial s_o} - \beta_o \frac{\partial \theta_o}{\partial n_o}\right)$$

$$F_2 = \frac{A_o}{M_o}\left[(\beta_o B - \theta_1)\frac{\partial p_o}{\partial s_o} - (C - \beta_o \theta_1)\frac{\partial p_o}{\partial n_o}\right] + \frac{\theta_1}{M_o}\left(\frac{\partial \theta_o}{\partial s_o} + \beta_o \frac{\partial \theta_o}{\partial n_o}\right)$$

$$G = \frac{\varphi_1 + \theta_1 \cos \theta_o}{M_o r}$$

$$A = \frac{\beta_o}{\gamma p_o M_o^2}$$

$$B = \frac{p_1}{p_o} + \frac{1}{\beta_o^2}\left(\frac{p_1}{p_o} - \frac{\rho_1}{\rho_o}\right)\left[1 + \frac{2}{(\gamma - 1)M_o^2}\right]$$

$$C = \frac{p_1}{p_o} - \left(\frac{p_1}{p_o} - \frac{\rho_1}{\rho_o}\right)\left[1 + \frac{2}{(\gamma - 1)M_o^2}\right]$$

One additional relation is needed to determine the density perturbation, ρ_1, which appears in the coefficients of equations (14). The usual approach is to introduce the entropy function

$$\frac{p}{\rho^{\gamma}} = \frac{p_{\infty}}{\rho_{\infty}^{\gamma}} e^{(S-S_{\infty})/c_v} \tag{16}$$

and apply the condition that the entropy remain constant on streamlines

$$\frac{\partial S}{\partial s} = 0 \tag{17}$$

The following first-order equation for density perturbation results when equation (16) is linearized

$$\rho_1 = \frac{\rho_o}{\gamma}\left(\frac{p_1}{p_o} - \frac{s_1}{c_v}\right) \tag{18}$$

and applying the transformation (6a) gives the needed equation for entropy perturbation

$$\frac{\partial S_1}{\partial s_o} = -\theta_1 \frac{dS_o}{dn_o} \tag{19}$$

The total derivative is used here since S_o is a function of n_o only. The enthalpy and temperature perturbations, though not necessary for the present analysis, may be obtained from the thermal and caloric equations of state. The result is

$$h_1 = c_p T_1 = c_p T_o \left(\frac{p_1}{p_o} - \frac{\rho_1}{\rho_o}\right) \tag{20}$$

Equations (13c), (15a,b), (18), and (19) are the set which will be integrated between the shock wave and the body surfaces subject to boundary conditions on these surfaces. These boundary conditions are derived in the next section.

Initial and Boundary Conditions

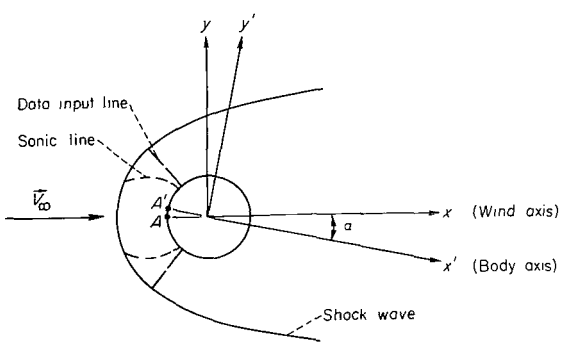

Sketch (b)

In the preceding analysis, use was made of the x,r,Φ coordinate system which is fixed with respect to the direction of the undisturbed stream (see fig. 1). It will be convenient from the computational standpoint to continue with this wind-oriented system. However, since the body axis system naturally enters the discussion of initial and boundary conditions, it is pertinent at this point to show the difference between these coordinate systems by means of a simple example. Consider the flow over a sphere at supersonic speeds, sketch (b).

As the body is rotated by angle α, an observer fixed with respect to $\vec{V}_\infty$ does not sense a change in the flow, whereas an observer fixed with the body does sense a change. This change can be computed from a knowledge of the axisymmetric flow field, and the equations for such a computation are derived in appendix B. These equations will be used in the specification of the boundary conditions below. Also, since it is usually desirable that final results be expressed in terms of body axes, this transformation is included as an option in the computer program described below.

Initial conditions.- In order to begin the computation of the flow field it is necessary to specify, along a line between the body and the shock, values for the four perturbation quantities p_1, ρ_1, θ_1, φ_1 and also the shock wave angle and position perturbations. (These quantities are introduced in the shock conditions below.) In the case of a blunt-nosed body, this initial-data line must be slightly downstream of the sonic line as shown in sketch (b). There is no restriction in the present analysis as to the nature of the body upstream of the initial-data line. For the general blunt-body flow, it may be possible to use the methods of reference 19, for example, to provide the necessary initial data. However, in the present application this problem is avoided by considering only spherically blunted or pointed bodies. For the spherically blunted body, all perturbation variables are initially zero. For the computation of flow over sharp-nosed bodies, initial values may be obtained from tabulated results for cone flow (ref. 4) or from a direct calculation of cone flow by the present methods.

Body conditions.- Two conditions at the body surface specify (1) the flow angle, θ, and (2) the entropy, S, at the surface. The prescribed value, θ_B, of the flow angle is given by the body geometry, while the entropy, S_B, depends on the angle of the shock wave through which the surface streamline passes. The problem at hand is to obtain the appropriate conditions on the perturbation quantities θ_1 and S_1. These conditions can be derived directly in terms of wind axes. However, it is simpler to work first with body axes and then apply the transformations given in appendix B to convert the results to wind axes.

The usual expansion procedure can be used to write the body conditions as follows in terms of body-axis (primed) variables

$$\theta_0 + \alpha\theta_1' \cos \Phi' = \theta_B \tag{21}$$

$$S_0 + \alpha S_1' \cos \Phi' = S_B \tag{22}$$

It is immediately evident for the flow angle that

$$\theta_1' = 0 \tag{23}$$

because the body angle cannot change and $\theta_o = \theta_B$. Specification of the entropy condition is more complicated since, for the general blunt body, the entropy perturbation at the surface may depend on the nose shape (see ref. 19). While this does not present any difficulty for the present method, nothing detailed can be stated about the general case until such blunt-body solutions are available. However, the entropy condition can be established for two specific cases of interest: (1) spherically blunted bodies and (2) pointed bodies. For the spherical nose, the surface entropy does not change for small angles of yaw, and therefore

$$S_1' = 0 \qquad \text{(spherical nose)} \tag{24a}$$

For pointed bodies, the entropy is constant along meridional planes, Φ' = constant. Then

$$S_1' = S_{1c} \qquad \text{(pointed nose)} \tag{24b}$$

where S_{1c} is the entropy perturbation obtained from the solution for a yawed cone. This latter condition seems to contradict the notion that the body surface should have a single value of entropy for all values of Φ'. It is pointed out in reference 8 that the entropy variation with Φ' is valid only outside a very thin "vortical" layer which is close to the body surface; also, it is stated that the pressure does not change across the thin layer. Therefore, equation (24b) is taken to be the proper condition for the "outer" flow. It is worth noting that in reference 20 it was concluded that this vortical layer could be neglected when the boundary layer on a yawed cone was studied.

The final step in obtaining the surface conditions is the conversion of equations (23) and (24) into the wind-axis system. This is done with the use of equations (B4) and (B16). The result is

$$\theta_1 = -1 + x \frac{\partial \theta_o}{\partial r} - r \frac{\partial \theta_o}{\partial x} \tag{25}$$

and

$$S_1 = K + x \frac{\partial S_o}{\partial r} - r \frac{\partial S_o}{\partial x} \tag{26}$$

where

$$K = \begin{cases} 0, & \text{spherical nose} \\ S_{1c}, & \text{pointed nose} \end{cases}$$

Since the entropy, S_o, is a function of the normal coordinate, n_o, only equation (26) may be written as

$$S_1 = K - (x \sin \theta_o + r \cos \theta_o) \frac{dS_o}{dn_o} \tag{27}$$

Equations (25) and (27) provide the desired body conditions, so attention is now directed to the boundary conditions at the shock wave.

Shock conditions.- The conditions on pressure, density, and flow-angle perturbations will be derived first with the use of wind coordinates. The procedure initially follows that of reference 14 in that the shock wave locus is expanded in terms of the usual series for α and Φ. However, since the jump conditions are conveniently expressed in terms of shock-wave angle, σ, this parameter is also introduced in the present analysis. With use of the notation shown in sketch (c), the shock position and angle are written in the following linearized form:

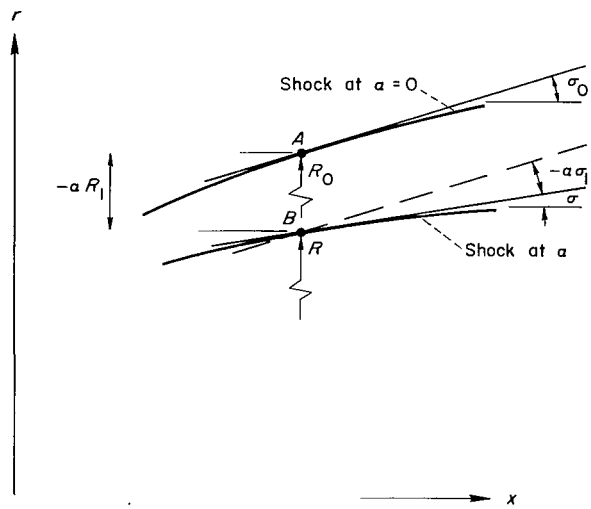

Sketch (c)

$$R(x,\Phi;\alpha) = R_0(x) + \alpha R_1(x)\cos\Phi \qquad (28)$$

$$\sigma(x,\Phi;\alpha) = \sigma_0(x) + \alpha\sigma_1(x)\cos\Phi \qquad (29)$$

If one imagines a cone tangent to the shock at point A, the angle perturbation, σ_1, is easily recognized as the ratio of shock to body yaw angles. The two shock perturbation parameters, that will appear in the boundary conditions, are unknown functions which must be specified initially and computed point by point along the shock surface. To this end, an additional equation is available which relates R_1 to σ_1. This is obtained from the geometrical relation

$$\frac{dR}{dx} = \tan\sigma \qquad (30)$$

Using equations (28) and (29) results in

$$\frac{dR_1}{dx} = \sigma_1 \sec^2\sigma_0 \qquad (31)$$

The problem now is to specify p_1, ρ_1, θ_1, and φ_1 in terms of R_1, σ_1, and the jump conditions (it is more straightforward here to work with density rather than entropy). The first three of these variables are considered in the next paragraph and the crossflow angle will follow.

Conditions on p_1, ρ_1, and θ_1: For uniform free-stream conditions, the conditions immediately behind the shock are functions of σ only and, hence, may be expanded in series as follows. (The analysis is given for pressure only, but holds also for density and flow angle with change of notation.)

$$p_S = p_{S_o} + \frac{dp}{d\alpha}\alpha + \ldots = p_{S_o} + \frac{dp}{d\sigma}\frac{d\sigma}{d\alpha}\alpha + \ldots \tag{32}$$

Here, $d\sigma/d\alpha$ is shock-angle perturbation, σ_α, and $dp/d\sigma$ can be evaluated in terms of the oblique shock relations (see, e.g., ref. 21). In equation (32), p_S is the pressure behind the yawed shock (point B, sketch (c)). For the present problem, however, the calculations are made along the characteristics of the axisymmetric field, and therefore the pressure perturbation at point A must be specified. This can be done by expanding the pressure in terms of radial distance from point A.

$$p_S = p_B = p_A + \left(\frac{\partial p}{\partial r}\right)_A (R_B - R_A) + O(\alpha^2) \tag{33}$$

By substitution of equation (33) into (32), and with the use of equations (28) and (29), the boundary condition on p_1 is obtained

$$p_1 = \sigma_1 \left(\frac{dp}{d\sigma}\right) - R_1 \left(\frac{\partial p_o}{\partial r}\right) \tag{34}$$

Similarly, for the density and flow angle

$$\rho_1 = \sigma_1 \left(\frac{d\rho}{d\sigma}\right) - R_1 \left(\frac{\partial \rho_o}{\partial r}\right) \tag{35}$$

$$\theta_1 = \sigma_1 \left(\frac{d\theta}{d\sigma}\right) - R_1 \left(\frac{\partial \theta_o}{\partial r}\right) \tag{36}$$

For a perfect gas, the derivatives with respect to shock angle are

$$\frac{dp}{d\sigma} = \frac{4\gamma}{\gamma + 1} p_\infty M_\infty^2 \sin \sigma_o \cos \sigma_o \tag{37}$$

$$\frac{d\rho}{d\sigma} = 2\rho_o \left\{\cot \sigma_o - \frac{\sin \sigma_o \cos \sigma_o}{\sin^2 \sigma_o + [2/(\gamma - 1)M_\infty^2]}\right\} \tag{38}$$

$$\frac{d\theta}{d\sigma} = 1 - \frac{\sin(\sigma_o - \theta_o)\cos(\sigma_o - \theta_o)}{\sin \sigma_o \cos \sigma_o} + \frac{4 \cos^2(\sigma_o - \theta_o)}{(\gamma + 1)M_\infty^2 \sin^2 \sigma_o} \tag{39}$$

Condition on φ_1: The shock condition for crossflow angle φ_1 is obtained from the conservation of tangential momentum in the azimuthal plane

of the shock wave. For the application of this condition it is helpful to use a shock-oriented coordinate system, and to consider the cone tangent to the shock shown in sketch (d). The cone is yawed by the angle $-\alpha\sigma_1$. Conservation of tangential momentum across the shock requires that

$$w'' = \vec{V}_\infty \cdot \vec{e}_t \qquad (40)$$

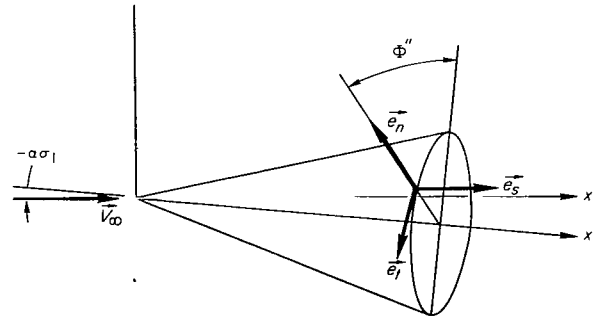

Sketch (d)

Here $\vec{e}_t$ is a unit vector oriented in the azimuthal direction with respect to the shock (sketch (d)), w'' is the velocity component in the $\vec{e}_t$ direction, and the double prime indicates a shock-oriented coordinate system. For the plane $\Phi'' = \pi/2$, the component of $\vec{V}_\infty$ along $\vec{e}_t$ is $-V_\infty \sin(-\alpha\sigma_1)$, and therefore the scalar product in equation (40) gives, in the general case,

$$\vec{V}_\infty \cdot \vec{e}_t = V_\infty \alpha\sigma_1 \sin \Phi'' \qquad (41)$$

Thus,

$$\varphi_1'' = \frac{w_1''}{V_o} = \frac{V_\infty}{V_o}\,\sigma_1 \qquad (42)$$

Now, in order to convert the above condition into wind axes, the transformations developed in appendix B can be used. Equation (B17) applies here except for the factor $-\sigma_1$, since $-\alpha\sigma_1$ is the rotation angle for the present case. Therefore the equation which must be used here is

$$\varphi_1 = \varphi_1'' - \sigma_1 \left(\cos \theta_o - \frac{x}{r} \sin \theta_o\right) \qquad (43)$$

(Equation (B4) need not be considered since $\varphi_o = 0$.) The boundary condition on crossflow angle is therefore

$$\varphi_1 = \sigma_1 \left(\frac{V_\infty}{V_o} - \cos \theta_o + \frac{x}{r} \sin \theta_o\right) \qquad (44)$$

This completes the specification of the equations and boundary conditions of the problem. Attention is now directed to a brief description of the computer program written for the solution of the equations and to some of the results obtained from the program.

NUMERICAL COMPUTATIONS

Equations and boundary conditions for the first-order-perturbation flow field have been presented in the previous sections. The solution of

these equations by the method of characteristics was programmed, in FORTRAN machine language, for the IBM 7090 computer. Since the solution of the first-order problem required a detailed knowledge of the zero-order (zero angle of yaw) flow field, the perturbation program was incorporated into an existing program for axisymmetric flow (ref. 3). This program was modified to compute perturbation quantities at each mesh point, after the zero-order quantities had been computed. Pertinent aspects of the computer program, as modified, are described below, followed by a presentation of some results.

Computer Program

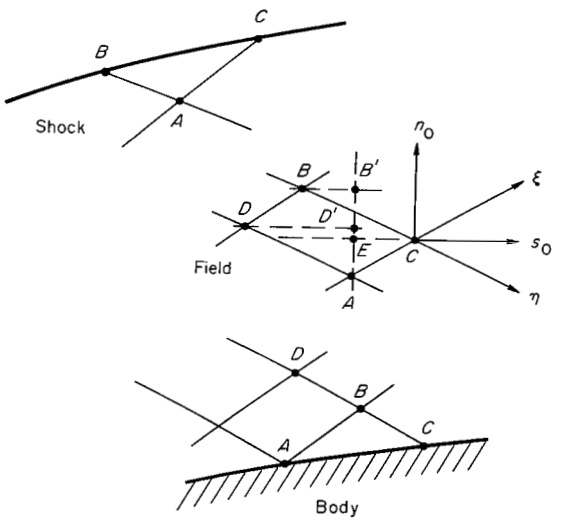

Sketch (e)

The basic computing unit of the program involves mesh points A, B, and C shown in sketch (e) for body, field, and shock points. The compatibility and boundary conditions are used in the usual manner to determine data at point C in terms of known data at points A and B. A fourth point, D, is used in the body and field calculations in order to obtain a quadratic interpolation for certain variables as explained below. The procedure for the perturbation problem differs from that for axisymmetric flow in that (1) gradients of zero-order quantities must be computed and (2) the entropy perturbation and crossflow angle must be integrated along the streamline direction, s_o. These two points are discussed next.

Gradients of the axisymmetric field.- A linear, backward difference method is used to compute the gradients of pressure, p_o, and flow angle, θ_o, along the characteristic directions for field points, and along characteristic and boundary directions for boundary points. Thus, for example, from the difference of data at points A and C, gradients are obtained which are applied to point C. The gradients obtained in this manner for two oblique directions are then transformed to components in the s_o and n_o directions for use in the calculations.

At body and field points, entropy is approximated by a second-degree polynomial in the normal coordinate with the use of data at points A, B, and D (sketch (e)). The gradient thus obtained is applied at point C. For the shock point, the entropy gradient is obtained by a linear approximation.

At the body, the pressure gradient in the normal direction, $\partial p_o/n_o$, is computed directly from the momentum equation (1b) and the boundary condition on θ_o.

Calculation for φ_1 and S_1.- The equations for crossflow angle and entropy perturbations (eqs. (13c) and (19)) involve the derivative of these quantities with respect to s_o only. These quantities are, in general, functions of both s_o and n_o, and therefore the equations apply along a line n_o = constant. The problem which arises in the numerical computation is that the field points A, B, C, and D do not correspond to the same value of n_o (see sketch (e)). This problem is resolved in the following manner. With the use of slopes defined by equations (13c) and (19), the data at B and D are projected forward, in the s_o direction, to the line AB'. The variables φ_1 and S_1 are then evaluated at point E by means of quadratic interpolation with data at points A, D', and B'. Evaluation of these variables at point C is then completed with the help, once again, of equations (13c) and (19) and the data at point E.

Input data.- The computer program requires input information giving free-stream conditions, and starting data at as many as 40 points along a noncharacteristic line between the body and the shock. These data include (1) starting values x, r, V, θ, p, and ρ for the axisymmetric flow, and (2) the first-order perturbation quantities V_1, θ_1, φ_1, p_1, and ρ_1. For the results presented herein, these starting data were derived in the following manner.

For the pointed body, starting data was obtained from a solution for the flow over the tangent cone to the pointed nose. While some such solutions are tabulated in reference 5, the cone angles and Mach numbers are limited. Therefore, in order to provide for arbitrary conditions, the methods presently being described were specialized to the cone problem. The somewhat simplified equations were then programmed to provide solutions to cone flow, and these results were used for input to the general program. The results of this cone program are compared with those of reference 5 in the following section.

For the blunt-nosed bodies, starting values for the axisymmetric flow were obtained from a computer program based on the inverse method of references 1 and 2. Since the blunt-body results presented are restricted to spherical-nosed bodies, all starting perturbation quantities were set equal to zero.

Specification of initial data as described above permits the present computer programs to be used for the computation of flows over pointed, or spherically blunted bodies of revolution at small angles of yaw. A number of these flows were obtained, and some of the results are presented in the next section with the object of establishing the accuracy and range of applicability of the linearized characteristics method.

Results

The computer programs described herein make it possible to obtain the detailed flow fields over particular bodies with a small manual effort and, therefore, a detailed presentation or tabulation of results is not attempted. However, in order that the computer programs may be used with confidence, this

section will present results which are intended to show the accuracy and range of applicability of the method. It is important to recall that the perturbation variables obtained from the present solution are, strictly speaking, derivatives with respect to yaw angle as defined by equations (3) and (4). Specifically, the perturbation variables shown in the following results may be written

$$\left.\begin{aligned} p_1 &= \frac{1}{\cos \Phi}\left(\frac{\partial p}{\partial \alpha}\right)_{\alpha=0} \\ \theta_1 &= \frac{1}{\cos \Phi}\left(\frac{\partial \theta}{\partial \alpha}\right)_{\alpha=0} \\ \rho_1 &= \frac{1}{\cos \Phi}\left(\frac{\partial \rho}{\partial \alpha}\right)_{\alpha=0} \\ \varphi_1 &= \frac{1}{\sin \Phi}\left(\frac{\partial \varphi}{\partial \alpha}\right)_{\alpha=0} \end{aligned}\right\} \tag{45}$$

and so on. Therefore, the applicability of the method depends primarily on the range of yaw angles over which a linear approximation may be used. Before this question can be answered, however, it is necessary to establish the accuracy of the numerical computations.

Accuracy of the numerical computations.- Two methods are used herein to assess the numerical accuracy: (1) a direct comparison with other numerical results, and (2) a self-comparison of the results obtained with various characteristic mesh sizes. The first check can, of course, be made only in particular cases. One such case is the yawed cone for which accurate tabulated results of reference 5 are available (note that corrections to the crossflow velocity given in reference 6 must be used with the tabular data). A computer program based on the present linearized characteristics method was written for the cone problem, and results of this program are shown in figure 3 together with the results of reference 5. First-order perturbations to the pressure, density, flow angle, and crossflow angle are presented for a 15° cone at two Mach numbers. It may be seen that the general form of the present solution agrees with that of reference 5 but that there are some small differences. The effect of mesh size on these differences was investigated by recomputing the high Mach number case with differing numbers of steps between the shock and body. This effect is shown in figure 4 where the reciprocal of the number of steps is plotted on the abscissa. The variation of the pressure perturbation is nearly linear and is easily extrapolated to zero mesh size which presumably is the exact value. This extrapolated pressure, labeled $p_1^{(\infty)}$, differs from the result of reference 5 by less than 0.1 percent, and is used to compute the relative error also shown in figure 4. The advantage of

computing the relative error in this way is that it can be applied when exact solutions are not available. Such is the case for the ogive which is presented next.

Figure 5 shows the axial variation of the surface pressure perturbation on a fineness ratio 3 ogive at a Mach number of 5.05. Initial values for the ogive were obtained from the cone program; the starting tangent-cone was assumed to be 1 percent of the ogive length. Three solutions are shown in figure 5, corresponding to varying mesh sizes as controlled by the number of initial data points. Initial values of the surface pressure perturbation are the same for the three solutions, but numerical errors which depend on mesh size are introduced at downstream points. Figure 6 shows the effect of the mesh size on the surface pressure perturbation and the relative error at two body stations. For the finest mesh presented, the relative error is less than 4 percent; computing time on the IBM 7090 was approximately 10 minutes for this case.

Attention is now directed to a typical blunt-nosed body. Figure 7 shows the axial variation of surface pressure perturbation on a 15° sphere-cone at a Mach number of 10. This figure, as in the previous example, presents results for three solutions corresponding to different mesh sizes. These solutions are in reasonable agreement, and it is noted that they approach the cone value at a large distance from the nose. (The pressure perturbation curve has a discontinuous slope at the point of juncture between the sphere and cone; regions with discontinuous slopes also appear at downstream points (x/R_b = 8, 17) which correspond to subsequent reflections of the Mach wave from the sphere-cone juncture. These regions are examined in greater detail below.) Figure 8 shows the variation of surface pressure and relative error with mesh size for two points, x/R_b = 0.67 and 6.1. The relative error is about 3 percent for the finest mesh size and computing time was about 8 minutes.

Comparison with another numerical solution.- In reference 14, results are presented for the perturbation flow field over a 10° sphere-cone at a Mach number of 15. The calculations of reference 14 were based on the linearized characteristics method and therefore provide the opportunity for a direct check of the present computer program. However, before making a comparison, it is necessary to discuss two points: (1) discontinuities in the solutions, and (2) the differences of results presented in terms of wind and body axes.

Discontinuous solutions to the perturbation flow field were also noted in reference 14, and a method for calculating these solutions was discussed in some detail; results were not presented, however. No attempt is made in the present paper to treat the discontinuous solutions analytically, but it can be shown numerically that the effects of a discontinuous curvature are localized. This is done by computing the flow over a body with a short transition curve between the sphere and cone segments. Such a body is shown in figure 9. If the end point of the transition curve is allowed to match a cone which is slightly displaced from the original one, it is possible to express the curve as a fifth-degree polynomial which provides continuity of the first two derivatives at the starting point and of the first four derivatives at

the end point. Figure 10(b) shows the pressure perturbation on this body in the transition region and in the region of the first Mach wave reflection. Figure 10(a) shows the pressure perturbation at the shock and the shock-angle perturbation in the region where the Mach line from the sphere-cone juncture reaches the shock. It is seen that the transition curve eliminates the discontinuity and that at some distance from this point the results are essentially the same for both cases. This shows that the primary effects of the discontinuous surface curvature are confined to limited regions of the flow field. It must be emphasized, however, that the discontinuous jumps in the pressure perturbation are a failing of the present expansion technique. From the practical standpoint this failure is of minor consequence since in actual flows the viscous boundary layer tends to smooth the discontinuous body curvature.

To illustrate the effects of the wind-axes to body-axes transformation, as discussed in appendix B, use is made of results for a 15° sphere-cone at a Mach number of 10. Figure 11(a) shows the pressure perturbation at the body and at the shock, and figure 11(b) shows the shock position and angular perturbations. In the part of the flow field outside the region of influence of the conical portion of the body, all perturbations are zero with respect to wind axes. Also, in this region the perturbations with respect to body axes are determined by the solution of the axisymmetric flow field. (see appendix B). Downstream from the Mach line originating at the sphere-cone juncture, a body-axis variable is obtained by a combination of the wind-axis variable and the additional term obtained from the axis transformation. The contributions of both terms are evident in figure 11.

With these points in mind attention is directed to a comparison with the results of reference 14. Some of these results are reproduced in figure 12 in addition to those of the present computer program. Figure 12(a) shows the pressure perturbation for the body and the shock. The two results agree in general trend, but there are sizable differences in the pressure perturbation both at the shock and body which seem larger than estimated numerical errors. In view of the discussion of the preceding paragraph, the difference in the shock-wave pressure is likely due to differences in the nonyaw solution. This could possibly account also for the disagreement in body pressures. Figure 12(b) shows the variation of the crossflow angle along the body and shock surfaces. At the shock for x greater than 7.5 the two results do not agree. A reason for the disagreement has not been definitely established; however, it seems to be a result of differences in the shock boundary condition. The discontinuity in the crossflow angle in the present solution follows directly from the boundary condition which was written in terms of the shock angular perturbation, σ_1. The variation of this parameter with axial distance is shown in figure 12(c). Reference 14 presents the shock radial perturbation (fig. 12(c)), but not the angular perturbation, and therefore cause of the difference in crossflow angle cannot be established with certainty. It is noted, however, that the present results seem somewhat more consistent with the over-all flow picture in that the solutions tend to the cone solution at a large distance from the nose.

To this point, the results presented have pertained primarily to the numerical accuracy of the computer program described herein. There remains, however, the question of applicability of the linearized characteristics method for predicting the flow field over bodies at small yaw angles. This topic is discussed next.

Applicability of the linearized-perturbation method.- Strictly applied, the present method yields only the initial slope of the flow variables with respect to yaw angle. However, such a linear approximation can in many cases provide useful results over a range of yaw angles. In order to estimate the range of angles over which the linear approximation may be applied, one must compare linearized results with experiment, exact theories, or with solutions of the second order perturbation problem. Since results of exact theories are not available for the problem at hand, this section will rely on comparisons with experiment and with shock-expansion methods which are applicable to pointed bodies (see refs. 16 and 18). Although the shock-expansion theory must be considered an approximate method, it does include second-order effects of the yaw angle and, therefore, provides a check on the range of applicability of the present method.

In reference 18 comparisons are made between the predictions of the shock-expansion method and experimental results for yawed ogives. Some of these results are reproduced in figure 13 which also shows the predictions of the present method. The theories and the experimental points are in reasonable agreement at $\alpha = 0$ and $\alpha = 5^{\circ}$. At $\alpha = 10^{\circ}$ the present method predicts pressure coefficients somewhat lower than predicted by shock-expansion theory. Both methods use cone flow for initial values, but second-order perturbations were included in the shock-expansion results while the present method uses only the linear term. Therefore, the difference between the two theories at $x/L = 0$ can be attributed to this second-order term. It may also be inferred that the difference at other body stations is due to this term.

The shock-expansion method is often used to predict lift- and moment-curve slopes for pointed bodies. However, for ogive-cylinder bodies the theory does not work well. For this reason the second-order shock-expansion theory was developed in reference 22. Initial slopes of the normal-force curve and center-of-pressure locations for an ogive-cylinder are shown in figure 14. It is seen that the present method generally agrees with second-order shock-expansion theory except for predicting the center of pressure of ogive-cylinders of large fineness ratios. The reason for this difference is difficult to assess with the present information (it cannot be attributed to second-order yaw effects since only initial slopes are involved).

For blunt-nosed bodies, the shock-expansion method is not applicable, and results of other sufficiently accurate theories are not available. However, unpublished experimental data which are ideally suited for such a comparison have been made available by Mr. Joseph W. Cleary of NASA. The data were obtained from the Ames 3.5-Foot Hypersonic Wind Tunnel and include surface pressure distributions on yawed spherically blunted cones. Figure 15 compares the predictions of the present method with some of this experimental data for 15° and 30° cones at a Mach number of about 10. For both cones, the

theory and experiment agree as well for 2° yaw as for zero yaw. However, for 5° yaw the agreement is better for the 30° than for the 15° cone. The disagreement at 5° yaw for the spherically blunted 15° cone is attributed primarily to second-order yaw effects which are neglected by the present theory.

In these comparisons with experiment it is seen that the accuracy of the linear approximation depends on the cone angle, and it might be anticipated to depend also on the Mach number. For blunt bodies, very little can presently be established concerning the dependence of the linear approximation on bluntness and Mach number. However, for slender bodies one can obtain some feel for these effects by applying hypersonic similarity concepts (e.g., refs. 16 and 23). Thus for slender bodies at large Mach numbers, similar flows are obtained if the parameters $K_T = M/f$ and $K_\alpha = M\alpha$ are unchanged. For these similar flows the error in the linear approximation depends on K_α only. Figure 16 shows conditions for flows which are similar to that for the ogive of figure 13, and these conditions show how the accuracy of the present method depends on Mach number and fineness ratio. Figure 16(a) indicates that for a fixed error the yaw angle must decrease with increasing Mach number, but that the fineness ratio must increase in order to obtain a similar flow. For both the error and the Mach number fixed, figure 16(b) shows that the yaw angle must decrease with increasing fineness ratio, a trend also noted in the blunt-body results of figure 15.

While the curves of figure 16 indicate how the error varies with fineness ratio, they do not show the Mach number variation for a fixed fineness ratio, nor do they provide a means for estimating its magnitude. For this purpose one can use second-order cone solutions. Figure 17 shows the ratio of the second- to first-order pressure perturbations as obtained from the tabulated results of reference 5 and from the thin-shock-layer theory of reference 24. Based on this ratio, the error in the linear approximation can be computed (neglecting higher order terms), and is shown on the ordinate of figure 17 for 2° yaw. It should be noted that this error is based upon the increment in pressure due to yaw, and that the percentages would be decreased if based upon the actual surface pressure.

For cone angles from about 5° to 45° Cheng's shock-layer theory and Kopal's numerical results both indicate a decrease in the error with increasing cone angle. The shock-layer theory passes through zero for a 45° cone and predicts increasing error for larger or smaller angles. For very small cone angles the approximations of shock-layer theory are violated and the decrease in error for cone angles less than 5° should be discounted. While the results of figure 17 are obtained for pointed cones they can, if used with caution, provide error estimates for blunted bodies. It is noted in the figure that the shock-layer theory approaches Newtonian theory for large Mach numbers, and therefore should provide error estimates for those conditions where the Newtonian approximation is applicable. The predicted decrease in error as the cone angle tends toward 45° is in agreement with the experimental results of figure 15 for sphere-cones.

Finally, it should be noted that for bodies of high fineness ratio a viscous crossflow (refs. 25 and 26) may become important. This viscous effect

is second order in angle of attack so that it has a variation with yaw angle which is essentially the same as that predicted by Newtonian theory. Recent experimental results on second-order viscous effects have also been obtained for cones in reference 27.

The first-order theory described herein provides the correct initial slope with respect to yaw, and is applicable so long as the second-order crossflow effects (inviscid or viscous) do not upset the linearity of the desired quantity (the lift curve, for example). The angle of yaw at which this occurs depends on the Mach number, the body slope, and on its over-all fineness ratio. A rule that has in the past been applied to pointed bodies states that the second-order yaw terms become important when the yaw angle approaches the half-angle of a cone tangent to the nose of the body.

CONCLUDING REMARKS

A computer program based on the linearized characteristics method was developed for calculating the supersonic portion of the flow of a perfect gas over arbitrary bodies of revolution at small yaw; a specialization of the general approach resulted, also, in a program which gives the first-order effects of yaw for pointed cones. First-order perturbation equations were derived in a form consistent with an existing method of characteristics computer program for the calculation of axisymmetric flows and the perturbation equations were incorporated into this program. This program was used to compute some example flows for establishing the accuracy and applicability of the method.

The results from the present method agreed with tabulated exact solutions for cone flow. Also, solutions for sphere-cone bodies tended to the cone solution at a large distance from the nose. An examination of the effect of mesh size on the results was made to establish the numerical accuracy of the results. Present solutions were then compared with published results for a 10° sphere-cone which had been computed by basically the same method. In general the results agreed, but some differences seemed greater than possible numerical errors. Some of the differences were attributed to the initial values obtained from the axisymmetric blunt-body solution for a sphere.

The applicability of the present method for predicting flows over bodies at finite yaw angles was assessed by comparison with experiment and, where possible, with other theories. For an ogive of fineness ratio 3, the results of the present method agreed with those from experiment and shock-expansion theory at yaw angles up to about 5°. For spherically blunted 15° and 30° cones, the present theory agreed well with experiment up to 2° yaw for the 15° cone and up to 5° yaw for the 30° cone. Estimates based on cone-flow theories indicate that for fixed yaw angle the error in the present linear approximation is least for 45° cones and increases for larger and smaller cone angles.

For slender pointed bodies, a practical rule which has been used, limits the present method to yaw angles less than the half-angle of the nose.

Ames Research Center
National Aeronautics and Space Administration
Moffett Field, Calif., March 3, 1964

APPENDIX A

INTRINSIC FORM OF THE EQUATIONS OF MOTION OF A PERFECT GAS FOR THREE-DIMENSIONAL FLOW

In development of the first-order perturbation equations it was found convenient to begin with the equations of motion written in terms of intrinsic coordinates, that is, coordinates consisting of the streamline and two of its normals. The equations in this form are given in reference 16 for axisymmetric flow. These are

$$\frac{\beta^2}{\rho V^2}\frac{\partial p}{\partial s} + \frac{\partial \theta}{\partial n} + \frac{\sin\theta}{r} = 0 \tag{A1a}$$

$$\frac{1}{\rho V^2}\frac{\partial p}{\partial n} + \frac{\partial \theta}{\partial s} = 0 \tag{A1b}$$

The problem at hand is to derive the analogous set of equations which are applicable to three-dimensional flow without axial symmetry. These will follow from the gas dynamics equation (i.e., combined momentum and continuity equations) and the momentum equation

$$a^2 \operatorname{div} \vec{V} - \vec{V} \cdot \operatorname{grad}\left(\frac{V^2}{2}\right) = 0 \tag{A2}$$

$$\frac{1}{\rho}\operatorname{grad} p + \operatorname{grad}\left(\frac{V^2}{2}\right) + \vec{V} \times \operatorname{curl} \vec{V} = 0 \tag{A3}$$

First, however, it is necessary to define the coordinate directions.

The streamline direction is uniquely defined in terms of the velocity vector, $\vec{V} = V\vec{s}$, and for two-dimensional flow the normal coordinate also is uniquely defined in terms of $\vec{V}$ (for axisymmetric flow $\vec{n}$ is in the meridional plane Φ = constant). However, in the three-dimensional case there are many possible normals to the velocity vector. One such possibility, which is not used here, is the normal which lies in the osculating plane and is called the principal normal to a curve. For the present perturbation problem it was found convenient to choose the normal $\vec{n}$ which lies in the meridional plane (fig. 1). The second normal, $\vec{t}$, is then uniquely defined in terms of $\vec{s}$ and $\vec{n}$. These unit vectors may be expressed in terms of two rotation angles by starting with the x_m, r_m, z_m axes shown in figure 1. This initial system of axes is rotated by angle θ about the z_m axis, and the resultant system is rotated by angle φ about $\vec{n}$; the angle θ is called the flow angle and φ the crossflow angle. If $\varphi = 0$, then $\vec{s}$ lies in the meridional plane and the normal $\vec{n}$ reduces to the usual normal for two-dimensional flow. With the

help of figure 1, these unit vectors may be easily written in terms of components in the x_m, r_m, z_m directions (i.e., in terms of unit vectors $\vec{e}_x$, $\vec{e}_r$, $\vec{e}_\Phi$).

$$\left.\begin{aligned} \vec{s} &= \cos\varphi\cos\theta\,\vec{e}_x + \cos\varphi\sin\theta\,\vec{e}_r + \sin\varphi\,\vec{e}_\Phi \\ \vec{n} &= -\sin\theta\,\vec{e}_x + \cos\theta\,\vec{e}_r \\ \vec{t} &= -\sin\varphi\cos\theta\,\vec{e}_x - \sin\theta\sin\varphi\,\vec{e}_r + \cos\varphi\,\vec{e}_\Phi \end{aligned}\right\} \qquad (A4)$$

Attention is now directed to the equations of motion (A2) and (A3). When the velocity vector $\vec{V}$ is eliminated in favor of $\vec{s}$, and the dot product of equation (A3) is taken first with $\vec{n}$ and then with $\vec{t}$, the following equations are obtained after some manipulation with vector identities

$$\frac{\beta^2}{\rho V^2}\,\vec{s}\cdot\operatorname{grad} p + \operatorname{div}\vec{s} = 0 \qquad (A5a)$$

$$\frac{1}{\rho V^2}\,\vec{n}\cdot\operatorname{grad} p + \vec{t}\cdot\operatorname{curl}\vec{s} = 0 \qquad (A5b)$$

$$\frac{1}{\rho V^2}\,\vec{t}\cdot\operatorname{grad} p - \vec{n}\cdot\operatorname{curl}\vec{s} = 0 \qquad (A5c)$$

These equations are the generalization of the intrinsic equations (A1) to general three-dimensional flow. To express them in the more familiar form of equations (A1) it is only necessary to expand the div and curl operators using the well-known vector formulas. To this end it is convenient to use equations (A4) and expand in terms of cylindrical coordinates (note that $(1/r)(\partial/\partial\Phi) = \cos\varphi(\partial/\partial t) + \sin\varphi(\partial/\partial s)$). The result is

$$\frac{\beta^2}{\rho V^2}\frac{\partial p}{\partial s} + \cos\varphi\frac{\partial\theta}{\partial n} + \frac{\partial\varphi}{\partial t} + \frac{\cos\varphi\sin\theta}{r} = 0 \qquad (A6a)$$

$$\frac{1}{\rho V^2}\frac{\partial p}{\partial n} + \cos\varphi\frac{\partial\theta}{\partial s} - \frac{\sin^2\varphi\cos\theta}{r} = 0 \qquad (A6b)$$

$$\frac{1}{\rho V^2}\frac{\partial p}{\partial t} + \frac{\partial\varphi}{\partial s} + \frac{\sin\varphi\sin\theta}{r} = 0 \qquad (A6c)$$

These equations can be simplified for flows which deviate by only a small degree from axisymmetric flow. Thus by making the usual linearizing approximations to the crossflow angle, the following equations of motion are obtained

$$\frac{\beta^2}{\rho V^2}\frac{\partial p}{\partial s} + \frac{\partial\theta}{\partial n} + \frac{\partial\varphi}{\partial t} + \frac{\sin\theta}{r} = 0 \qquad (A7a)$$

$$\frac{1}{\rho V^2}\frac{\partial p}{\partial n} + \frac{\partial \theta}{\partial s} = 0 \qquad \text{(A7b)}$$

$$\frac{1}{\rho V^2}\frac{\partial p}{\partial t} + \frac{\partial \varphi}{\partial s} + \varphi\frac{\sin\theta}{r} = 0 \qquad \text{(A7c)}$$

Equations (A7) are the desired generalizations of equations (A1), and are used for the development of the first-order perturbation equations.

APPENDIX B

EQUATIONS OF TRANSFORMATION FROM WIND TO BODY AXES

In the present development of the perturbation equations the need arises to change from variables expressed with respect to a wind-axis system to the corresponding variables expressed with respect to a body oriented system. The transformation equations giving this change are derived in this appendix first for scalar, and then for vector quantities. Consistent with the present analysis of the problem, these equations will give only the first-order effect in terms of a series expansion of the yaw angle. It is noted that such transformations were discussed in references 6 and 7 (including second-order terms) for use with the tabulated solutions for cone flow, reference 5.

SCALAR QUANTITIES

Consider any scalar quantity at a point (x,y) expressed as S(x,y) in wind-oriented coordinates and as S'(x',y') in the rotated (body) coordinates. Suppose now that point A in sketch (f) represents the location of a probe that is fixed with respect to the body at zero yaw. After rotation of the body by angle α, the probe will move to point B. Since a scalar can have only one value at a point regardless of the reference frame, that is, since

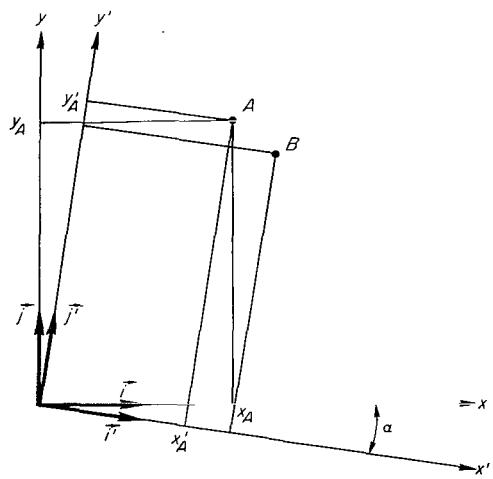

Sketch (f)

$$S(x,y) = S'(x',y') \qquad (B1)$$

the rotation is equivalent to a translation of the probe in the original reference frame. The desired transformation must therefore determine conditions at point B in terms of known conditions at point A. This is done by expanding S in a series about point A where it has the value $S(x_A,y_A)$. Thus

$$S'(x_B',y_B') = S'(x_A,y_A) = S(x_A,y_A) + (x_A - x_A')\frac{\partial S}{\partial x} + (y_A - y_A')\frac{\partial S}{\partial y} + \cdots \qquad (B2)$$

For small rotations, the prime coordinates are given by

$$\left.\begin{aligned} x' &= x - \alpha y \\ y' &= y + \alpha x \\ z' &= z \\ r' &= r + \alpha x \cos \Phi \end{aligned}\right\} \qquad \text{(B3)}$$

Substituting equations (B3) into (B2) and using the perturbation form

$$S = S_o + \alpha S_\alpha$$

yields the following equation which is valid to first order in α

$$S_\alpha'(x_A, y_A) = S_\alpha(x_A, y_A) + y_A \frac{\partial S_o}{\partial x} - x_A \frac{\partial S_o}{\partial y} \qquad \text{(B4)}$$

Equation (B4) states that the perturbation quantity S_α' at point A is given in terms of the value S_α at point A, plus an additional term proportional to the gradient of the axisymmetric field $S_o(x,y)$.

VECTOR QUANTITIES

In developing the axis transformation for vector quantities, the vectors are first expressed in terms of components along the same set of base vectors. These components can then be transformed according to equation (B4), developed for scalars. Consider the velocity vector with components u,v,w shown in sketch (g). The x',y',z' coordinate system is obtained by rotating x,y,z about the z axis. The velocity vector may be written in terms of components along wind and body axes as follows:

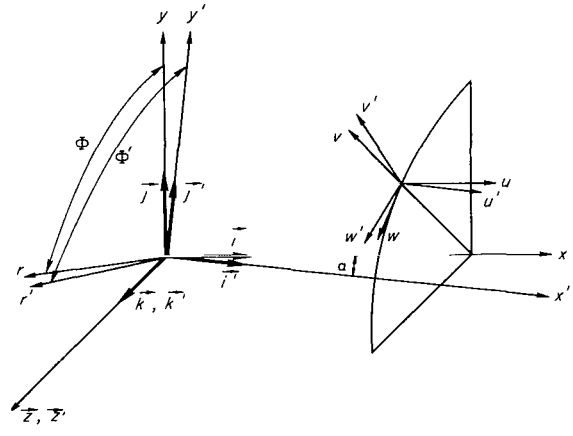

Sketch (g)

$$\vec{V}(x,r,\Phi) = u\vec{i} + (v \cos \Phi - w \sin \Phi)\vec{j} + (w \cos \Phi + v \sin \Phi)\vec{k} \qquad \text{(B5a)}$$

and

$$\vec{V}'(x',r',\Phi') = u'\vec{i}' + (v' \cos \Phi' - w' \sin \Phi')\vec{j}' + (w' \cos \Phi' + v' \sin \Phi')\vec{k}' \qquad \text{(B5b)}$$

where $\vec{i},\vec{j},\vec{k}$ are unit vectors along x,y,z axes and $\vec{i}',\vec{j}',\vec{k}'$ are along x',y',z' axes.

The vector, $\vec{V}$, can also be written in terms of components along the primed axes in the following manner.

$$\vec{V} = A\vec{i}' + B\vec{j}' + C\vec{k}' \tag{B6}$$

where

$$A = \vec{V} \cdot \vec{i}'$$

$$B = \vec{V} \cdot \vec{j}'$$

$$C = \vec{V} \cdot \vec{k}'$$

For small rotations the scalar products of the unit vectors are given by

$$\left.\begin{aligned} \vec{i} \cdot \vec{i}' = \vec{j} \cdot \vec{j}' = \vec{k} \cdot \vec{k}' = 1 \\ \vec{i} \cdot \vec{k}' = \vec{j} \cdot \vec{k}' = \vec{k} \cdot \vec{i}' = \vec{k} \cdot \vec{j}' = 0 \\ \vec{i} \cdot \vec{j}' = -\vec{j} \cdot \vec{i}' = \alpha \end{aligned}\right\} \tag{B7}$$

Equations (B5a) and (B7) can be used to write the components of equation (B6) in terms of unprimed variables:

$$\left.\begin{aligned} A &= u + \alpha(v \cos \Phi - w \sin \Phi) \\ B &= \alpha u + (v \cos \Phi - w \sin \Phi) \\ C &= (w \cos \Phi + v \sin \Phi) \end{aligned}\right\} \tag{B8}$$

The condition that the vector $\vec{V}$ be independent of the coordinate system

$$\vec{V}(x,y,\Phi) = \vec{V}'(x',y',\Phi') \tag{B9}$$

yields, upon equating coefficients of equations (B5b) and (B6), three scalar equations analogous to equation (B1). These are

$$\left.\begin{aligned} u - \alpha(v \cos \Phi - w \sin \Phi) &= u' \\ (v \cos \Phi - w \sin \Phi) + \alpha u &= (v' \cos \Phi' - w' \sin \Phi') \\ (w \cos \Phi + v \sin \Phi) &= (w' \cos \Phi' + v' \sin \Phi') \end{aligned}\right\} \tag{B10}$$

The angle Φ' may be written in terms of Φ by means of the usual expansions for small rotations, equations (B3), resulting in the following relations:

$$\cos \Phi' = \cos \Phi + \alpha \frac{x}{r} \sin^2 \Phi \tag{B11}$$

$$\sin \Phi' = \sin \Phi - \alpha \frac{x}{r} \sin \Phi \cos \Phi \tag{B12}$$

Now with equations (B11) and (B12) and the perturbation expansions

$$\left.\begin{aligned} u &= u_o + \alpha u_1 \cos \Phi \\ v &= v_o + \alpha v_1 \cos \Phi \\ w &= \alpha w_1 \sin \Phi \end{aligned}\right\} \tag{B13}$$

the following first-order equations are obtained from equations (B10)

$$u_1'(x',r') = -v_o(x,r) + u_1(x,r)$$

$$v_1'(x',r') = u_o(x,r) + v_1(x,r)$$

$$w_1'(x',r') = -u_o(x,r) + \frac{x}{r} v_o(x,r) + w_1(x,r)$$

Finally, application of equation (B4), which accounts for the gradient of the axisymmetric field, yields the following transformations for the vector components:

$$\left.\begin{aligned} u_1'(x,\ddot{r}) &= -v_o(x,r) + u_1(x,r) + y \frac{\partial u_o}{\partial x} - x \frac{\partial u_o}{\partial y} \\ v_1'(x,r) &= u_o(x,r) + v_1(x,r) + y \frac{\partial v_o}{\partial x} - x \frac{\partial v_o}{\partial y} \\ w_1'(x,r) &= -u_o(x,r) + \frac{x}{r} v_o(x,r) + w_1(x,r) \end{aligned}\right\} \tag{B14}$$

The corresponding expressions for angular variables may be obtained from equations (B14) and the definitions

$$\left.\begin{aligned} u_1 &= V_1 \cos \theta_o - \theta_1 V_o \sin \theta_o \\ w_1 &= V_o \varphi_1 \end{aligned}\right\} \tag{B15}$$

with the result

$$\theta_1' = 1 + \theta_1 + y \frac{\partial \theta_o}{\partial x} - x \frac{\partial \theta_o}{\partial y} \tag{B16}$$

and

$$\varphi_1' = \frac{x}{r} \sin \theta_o - \cos \theta_o \tag{B17}$$

REFERENCES

1. Van Dyke, Milton D., and Gordon, Helen D.: Supersonic Flow Past a Family of Blunt Axisymmetric Bodies. NASA TR R-1, 1959.

2. Fuller, Franklyn B.: Numerical Solutions for Supersonic Flow of an Ideal Gas Around Blunt Two-Dimensional Bodies. NASA TN D-791, 1961.

3. Inouye, Mamoru, and Lomax, Harvard: Comparison of Experimental and Numerical Results for the Flow of a Perfect Gas About Blunt-Nosed Bodies. NASA TN D-1426, 1962.

4. Stone, A. H.: On Supersonic Flow Past a Slightly Yawing Cone. Jour. Math. and Phys., vol. XXVII, no. 1, April 1948, pp. 67-81.

5. Staff of the Computing Section, Center of Analysis (Under Direction of Zdenek Kopal): Tables of Supersonic Flow Around Yawing Cones. Tech. Rep. 3, MIT, Cambridge, Mass., 1947.

6. Roberts, Richard C., and Riley, James D.: A Guide to the Use of the MIT Cone Tables. Jour. Aero. Sci., vol. 21, no. 5, May 1954, pp. 336-342.

7. Van Dyke, Milton D., Young, George B., and Siska, Charles: Proper Use of the MIT Tables for Supersonic Flow Past Inclined Cones. Readers' Forum, Jour. Aero. Sci., vol. 18, no. 5, May 1951, pp. 355-356.

8. Ferri, Antonio: Linearized Characteristics Methods. Ch. 6, sec. G of General Theory of High Speed Aerodynamics, W. R. Sears, ed., Princeton Univ. Press, Princeton, N. J., 1954, pp. 657-668.

9. Ferri, Antonio: The Method of Characteristics for the Determination of Supersonic Flow Over Bodies of Revolution at Small Angles of Attack. NACA Rep. 1044, 1951. (Supersedes NACA TN 1809)

10. Ferri, Antonio: The Linearized Characteristics Method and Its Application to Practical Nonlinear Supersonic Problems. NACA Rep. 1102, 1952. (Supersedes NACA TN 2515)

11. Ferrari, C.: Determination of the Pressure Exerted on Solid Bodies of Revolution With Pointed Noses Placed Obliquely in a Stream of Compressible Fluid at Supersonic Velocity. R. T. P. Translation No. 1105, British Ministry of Aircraft Production. (From Atti R. Accad. Sci. Torino, vol. 72, Nov. - Dec. 1936, pp. 140-163)

12. Sauer, Robert: Supersonic Flow About Projectile Heads of Arbitrary Shape at Small Incidence. R. T. P. Translation No. 1573, British Ministry of Aircraft Production. (From Luftfahrtforschung, vol. 19, no. 4, May 1942, pp. 148-152)

13. Forster, H. K.: Method of Characteristics for an Axially Symmetric Body Moving With Slight Yaw, and Application to the Corporal E Profile. JPL-CIT Progress Rep. 4-98, June 10, 1949.

14. Brong, E. A., and Edelfelt, I. H.: A Flow Field About a Spherically Blunted Body of Revolution at Small Yaw in a Hypersonic Stream. IAS 62-181, 1962.

15. Courant, R., and Friedrichs, K. O.: Supersonic Flow and Shock Waves. Interscience Pub., Inc., N. Y., 1948.

16. Hayes, Wallace D., and Probstein, Ronald F.: Hypersonic Flow Theory. Academic Press, N. Y., 1959.

17. Eggers, A. J., Jr., Syvertson, Clarence A., and Kraus, Samuel: A Study of Inviscid Flow About Airfoils at High Supersonic Speeds. NACA Rep. 1123, 1953. (Supersedes NACA TN 2646)

18. Eggers, A. J., Jr., and Savin, Raymond C.: A Unified Two-Dimensional Approach to the Calculation of Three-Dimensional Hypersonic Flows, With Application to Bodies of Revolution. NACA Rep. 1249, 1955.

19. Swigart, R. J.: A Theory of Asymmetric Hypersonic Blunt-Body Flows. AFOSR-TN-62-2232, Stanford Univ., (SUDAER No. 120), Jan. 1962.

20. Moore, Franklin K.: Laminar Boundary Layer on a Circular Cone in Supersonic Flow at a Small Angle of Attack. NACA TN 2521, 1951.

21. Ames Research Staff: Equations, Tables, and Charts for Compressible Flow. NACA Rep. 1135, 1953.

22. Syvertson, Clarence A., and Dennis, David H.: A Second Order Shock Expansion Method Applicable to Bodies of Revolution Near Zero Lift. NACA Rep. 1328, 1957.

23. Hamaker, Frank M., Neice, Stanford E., and Eggers, A. J.: The Similarity Law for Hypersonic Flow About Slender Three-Dimensional Shapes. NACA TN 2443, 1951.

24. Cheng, H. K.: Hypersonic Flows Past a Yawed Circular Cone and Other Pointed Bodies. Jour. Fluid Mech., vol. 12, pt. 2, Feb. 1962, pp. 169-191.

25. Van Dyke, Milton D.: First- and Second-Order Theory of Supersonic Flow Past Bodies of Revolution. Jour. Aero. Sci., vol. 18, no. 3 Mar. 1951, pp. 161-178, 216.

26. Allen, H. Julian: Pressure Distribution and Some Effects of Viscosity on Slender Inclined Bodies of Revolution. NACA TN 2044, 1950.

27. Tracy, Richard R.: Hypersonic Flow Over a Yawed Circular Cone. Calif. Inst. of Tech. Hypersonic Res. Proj. Memo. 69, Aug. 1, 1963.

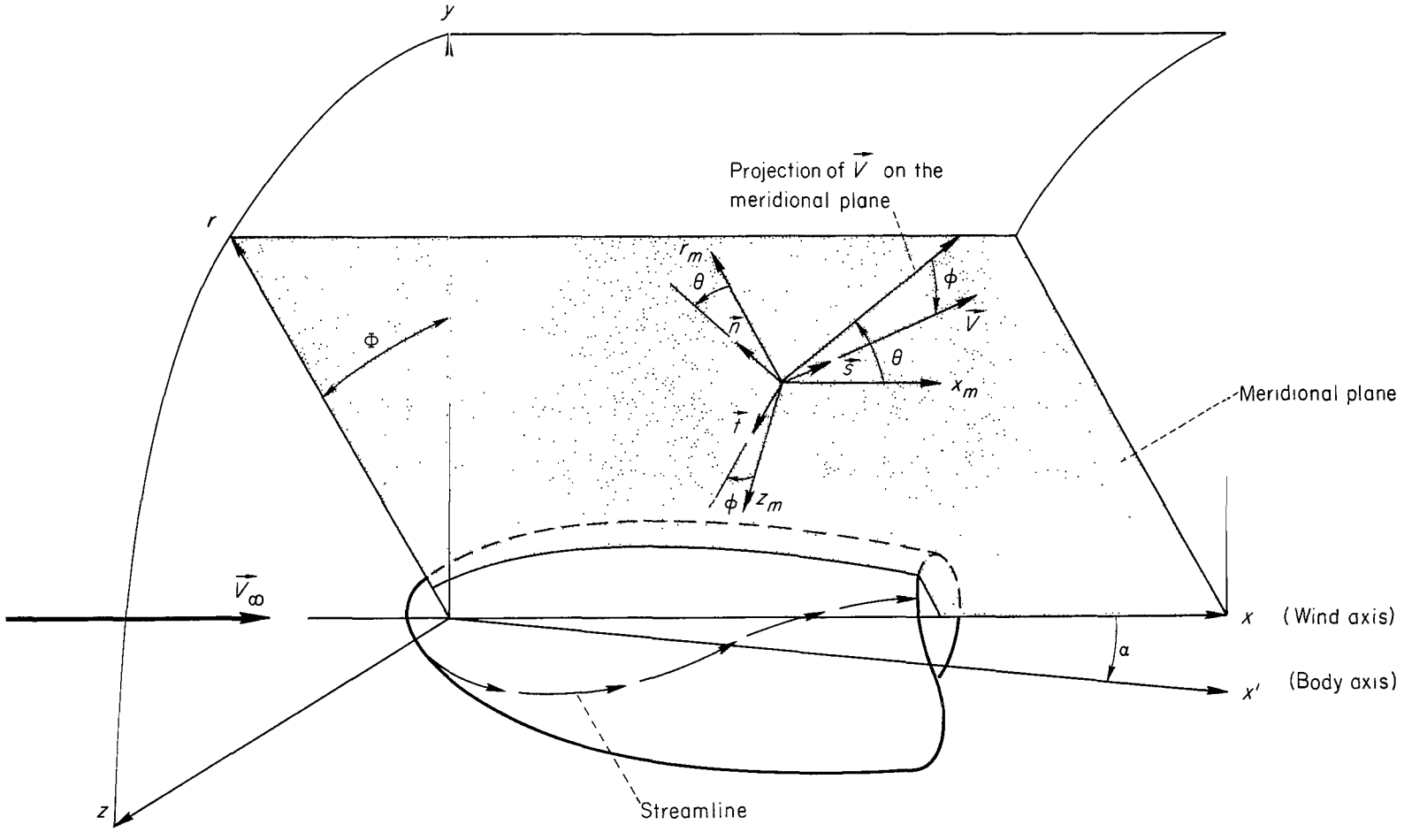

Figure 1.- Coordinate systems.

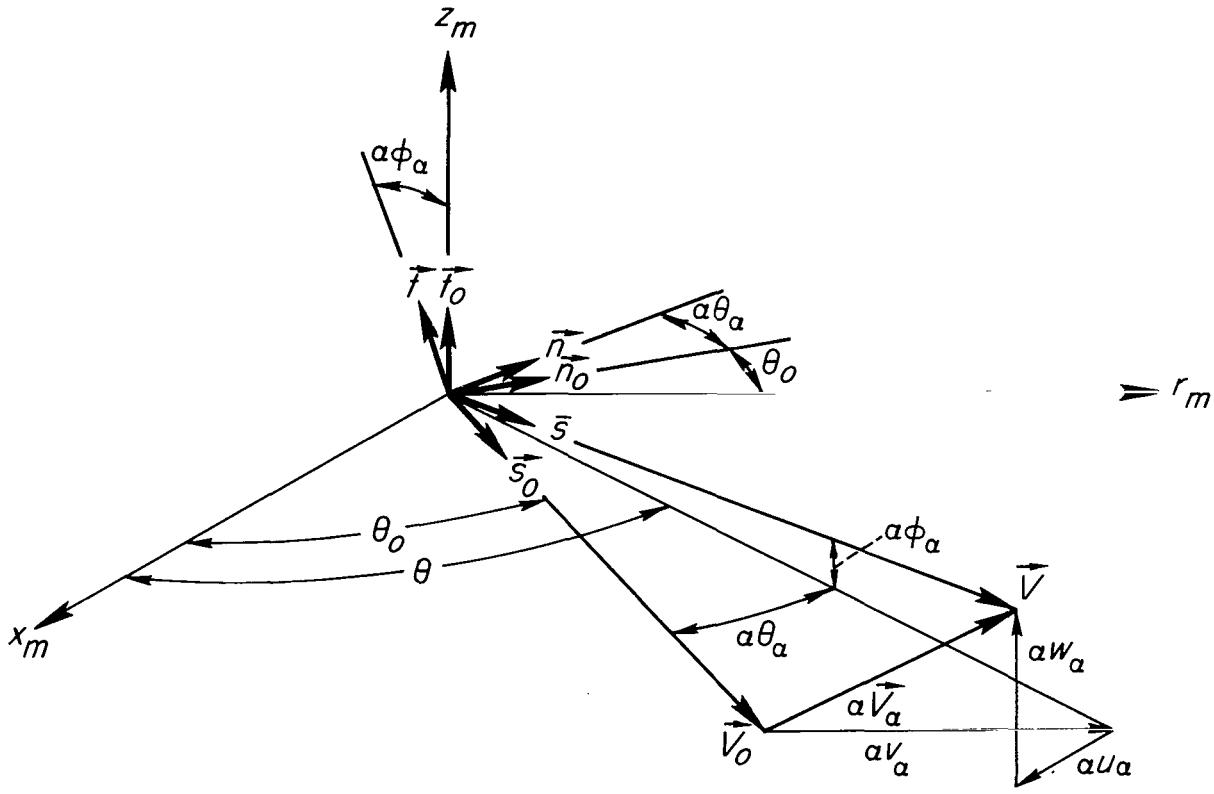

Figure 2.- Rotations defining the perturbation angles.

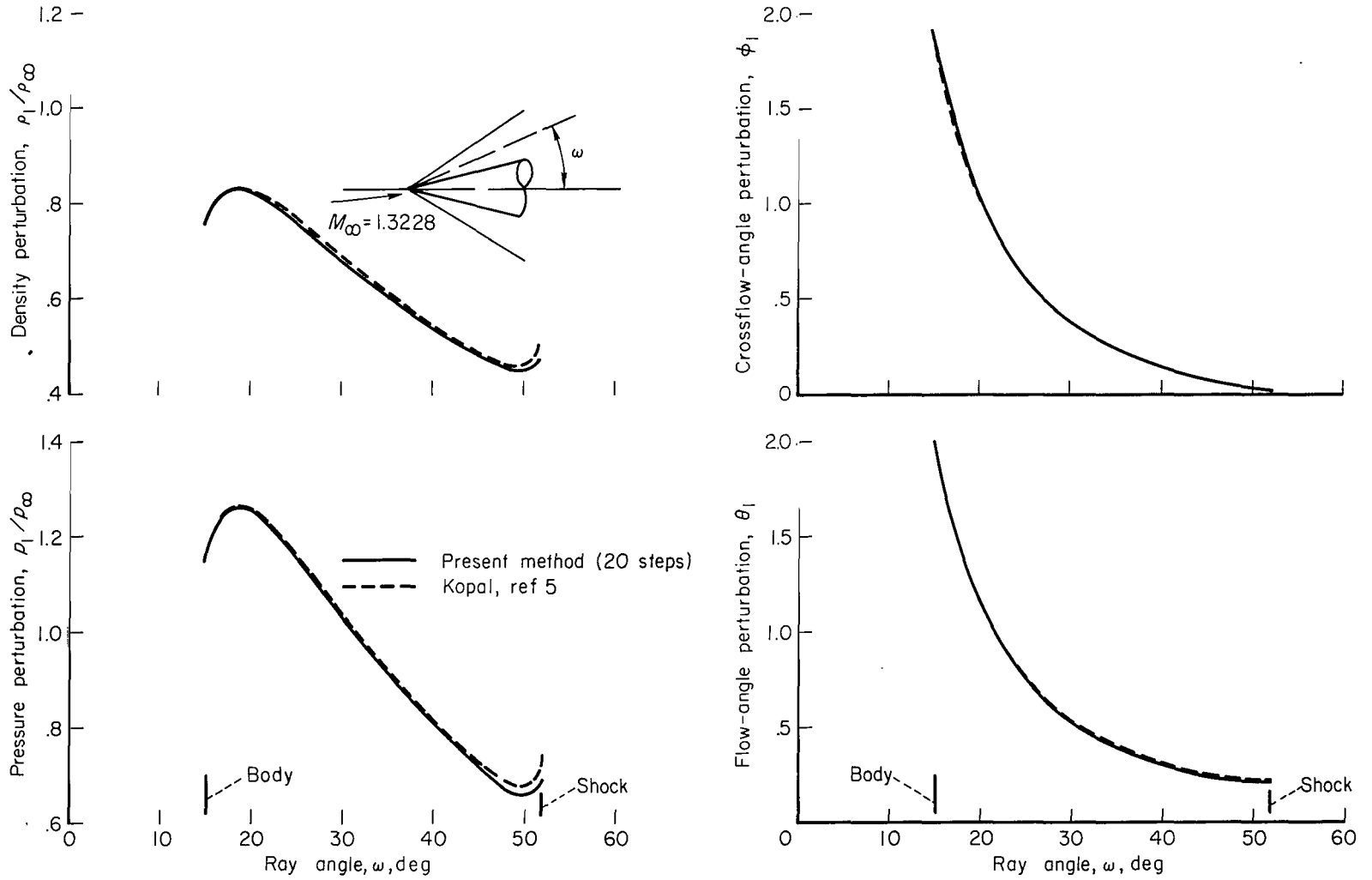

(a) $M_\infty = 1.3228$

Figure 3.- Variation of first-order perturbation variables in the flow field over a 15° cone (wind axes).

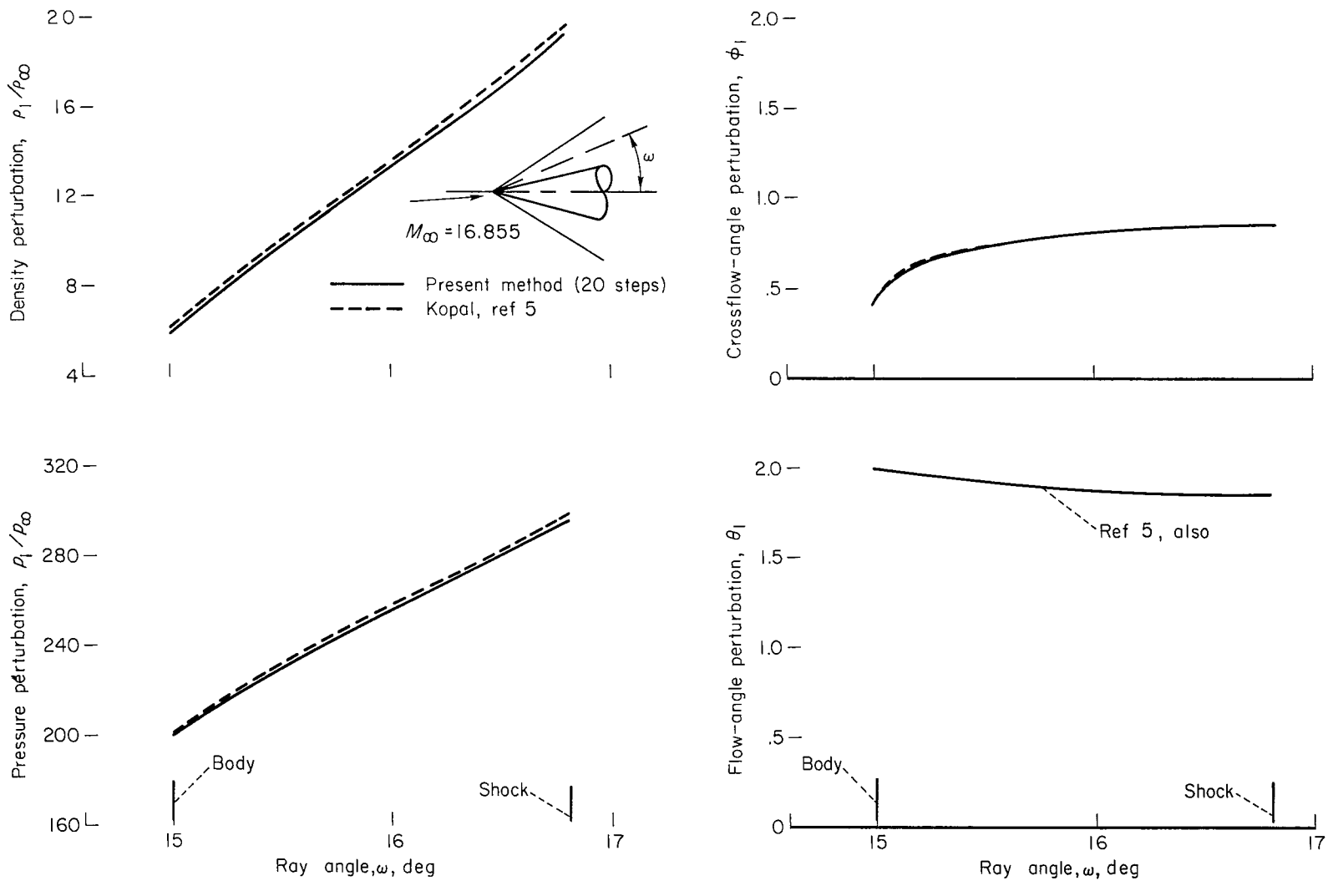

(b) M_∞ = 16.855

Figure 3.- Concluded.

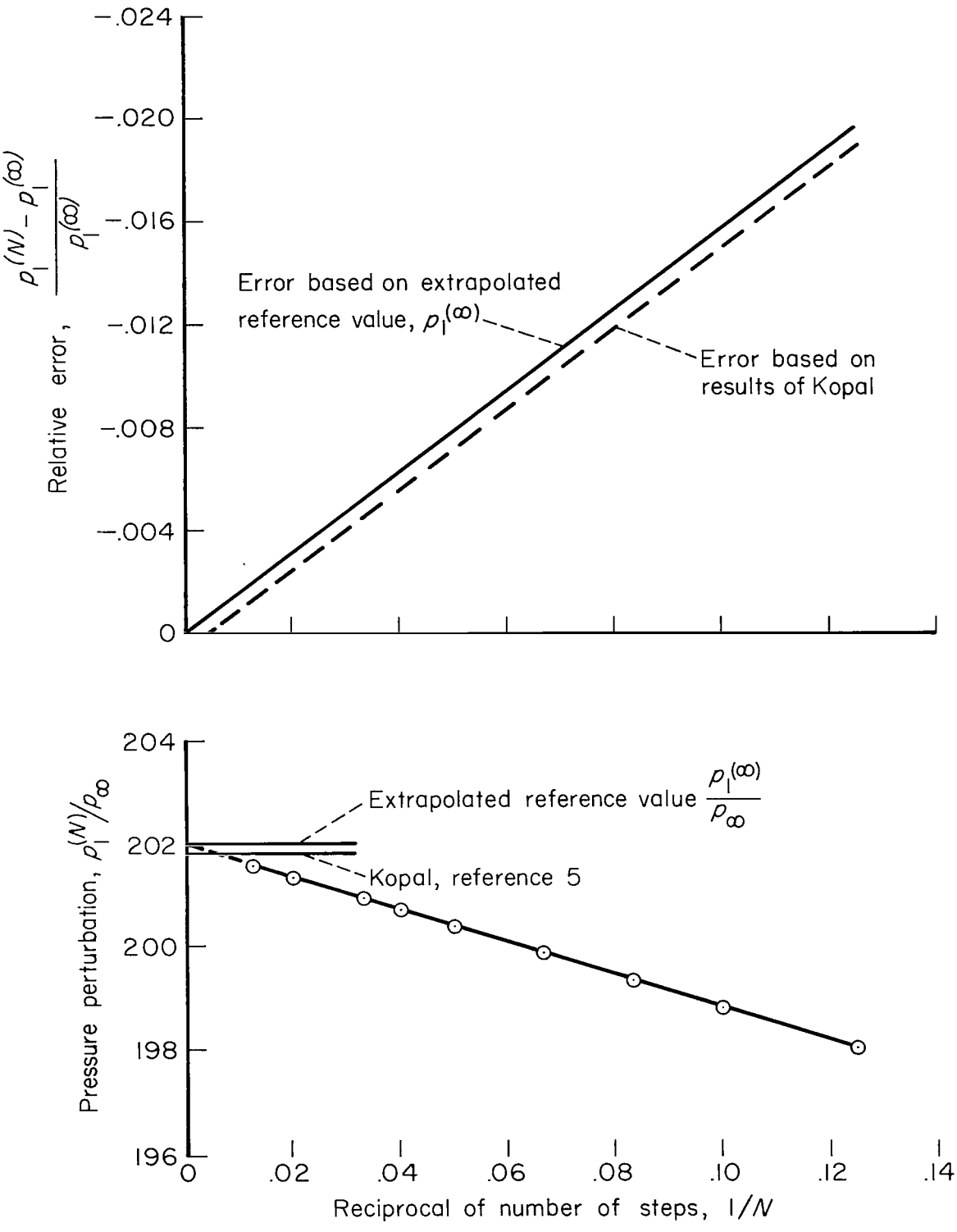

Figure 4.- Effect of mesh size on the accuracy of the surface pressure perturbation for a 15° cone; $M_\infty = 16.855$.

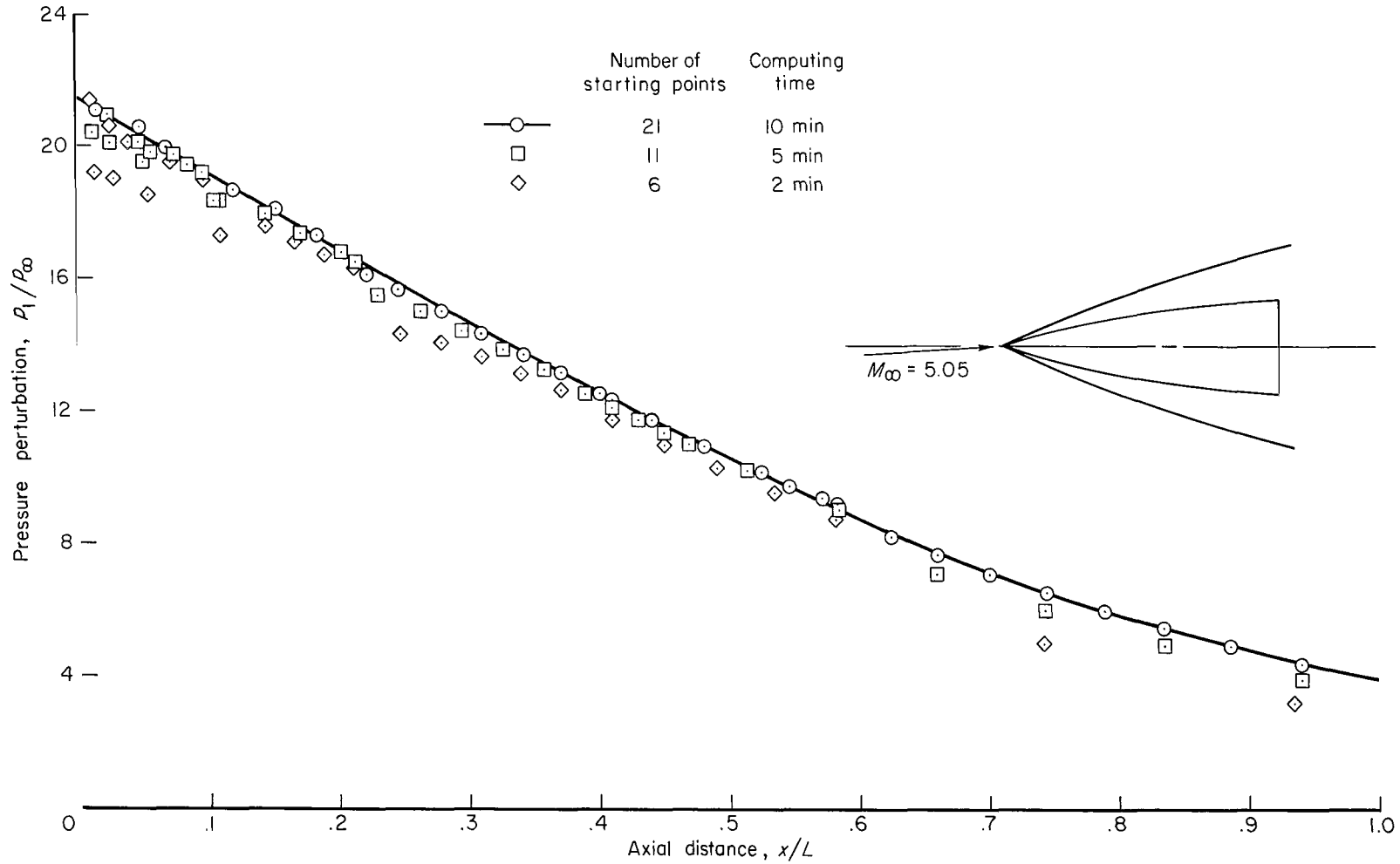

Figure 5.- Axial variation of surface pressure perturbation for an ogive of fineness ratio 3; M_∞ = 5.05 (body axes).

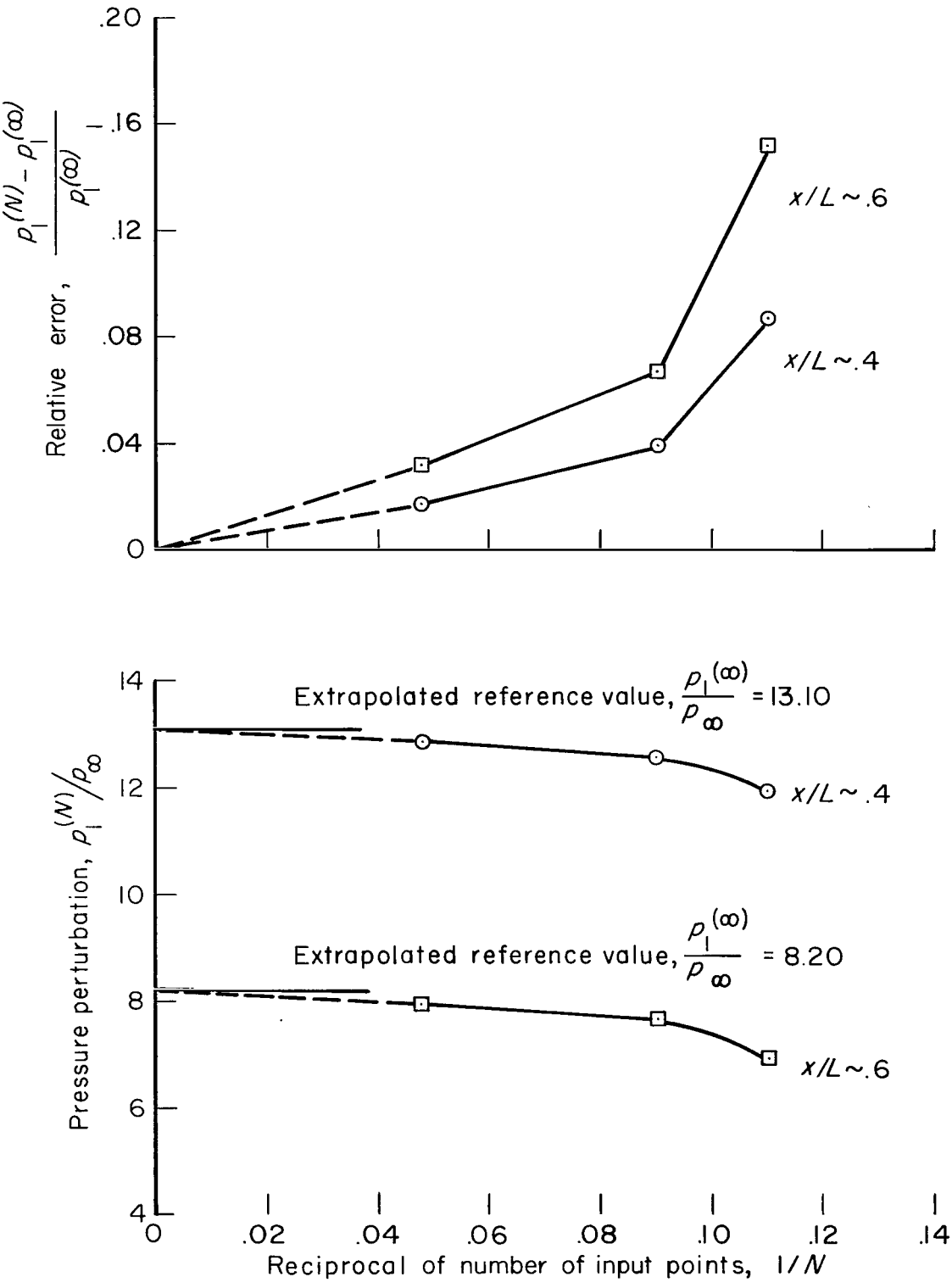

Figure 6.- Effect of mesh size on the accuracy of the surface pressure perturbation for an ogive of fineness ratio 3; $M_\infty = 5.05$.

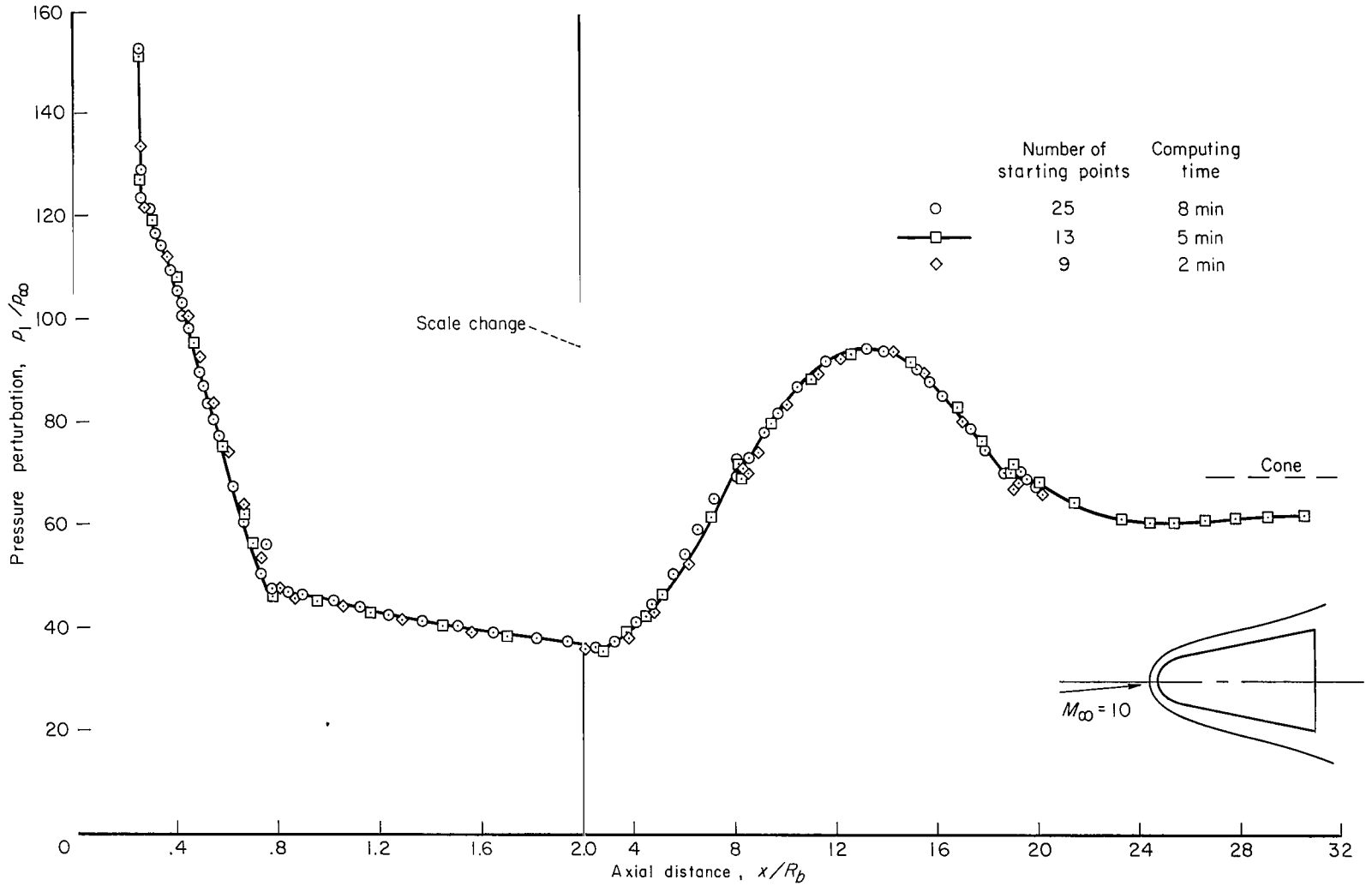

Figure 7.- Axial variation of the surface pressure perturbation for a spherically blunted 15° cone; M_∞ = 10 (body axes).

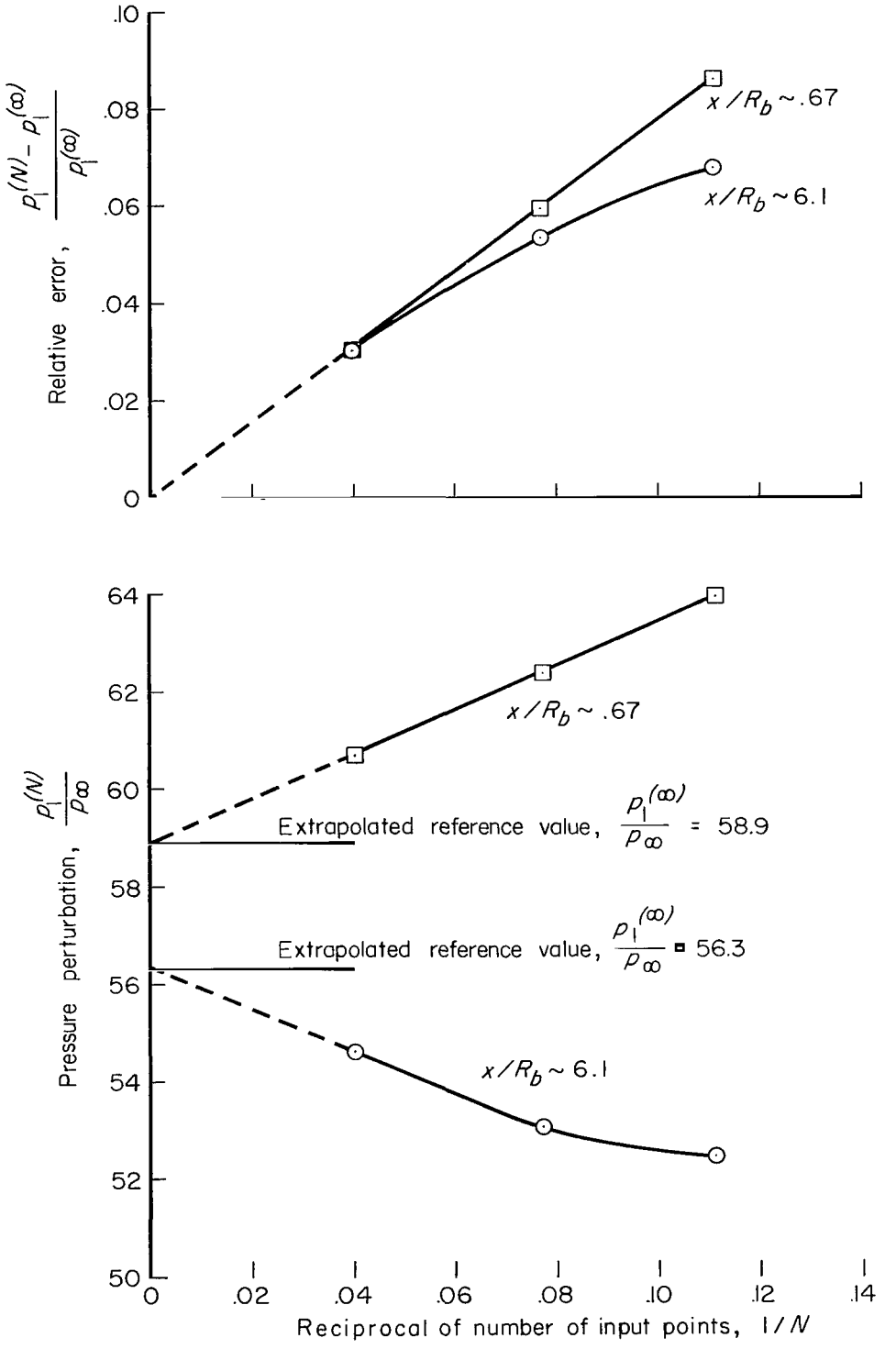

Figure 8.- Effect of mesh size on the accuracy of the surface pressure perturbation for a spherically blunted 15° cone; $M_\infty = 10$.

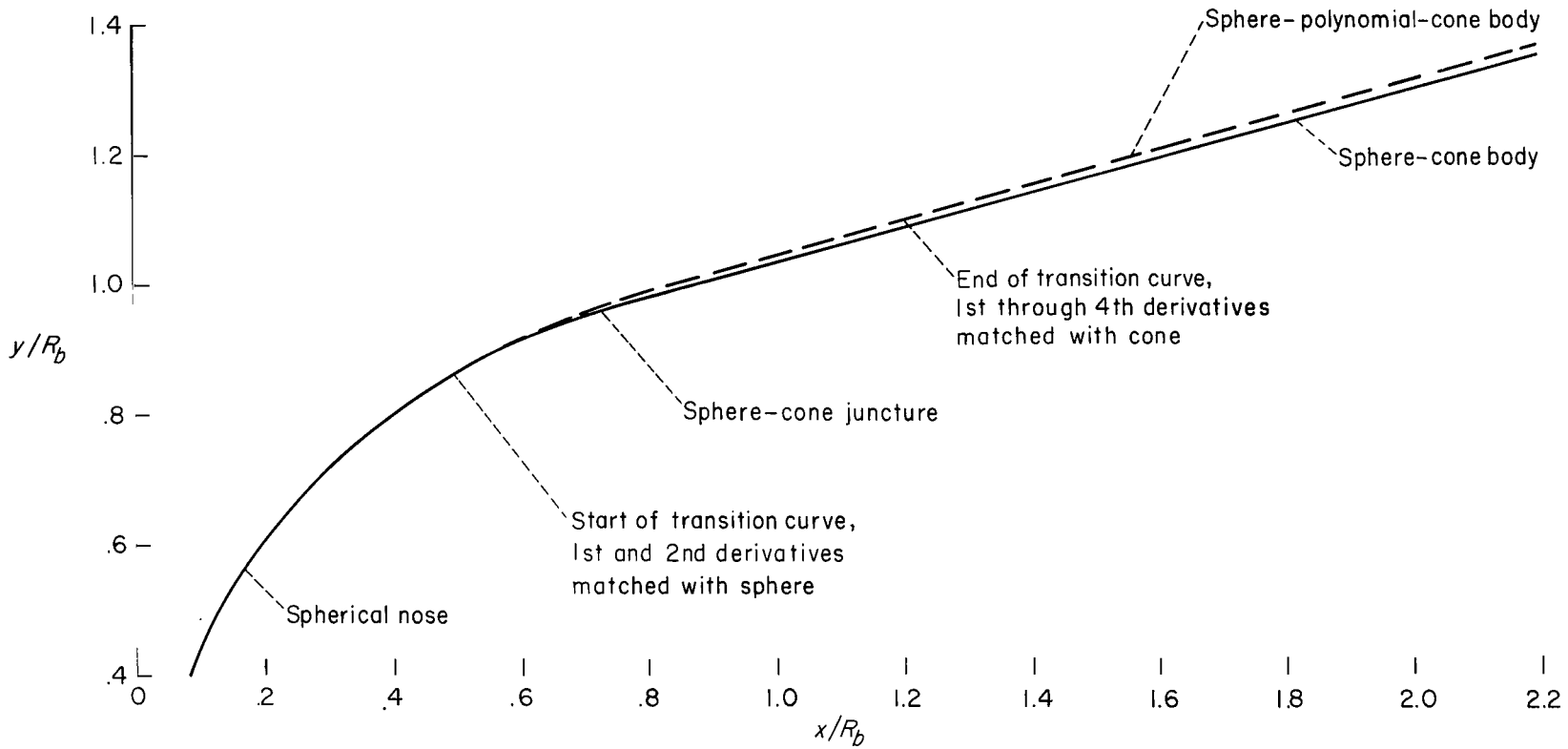

Figure 9.- Sphere-polynomial-cone body used to study the regions of discontinuous perturbation solutions.

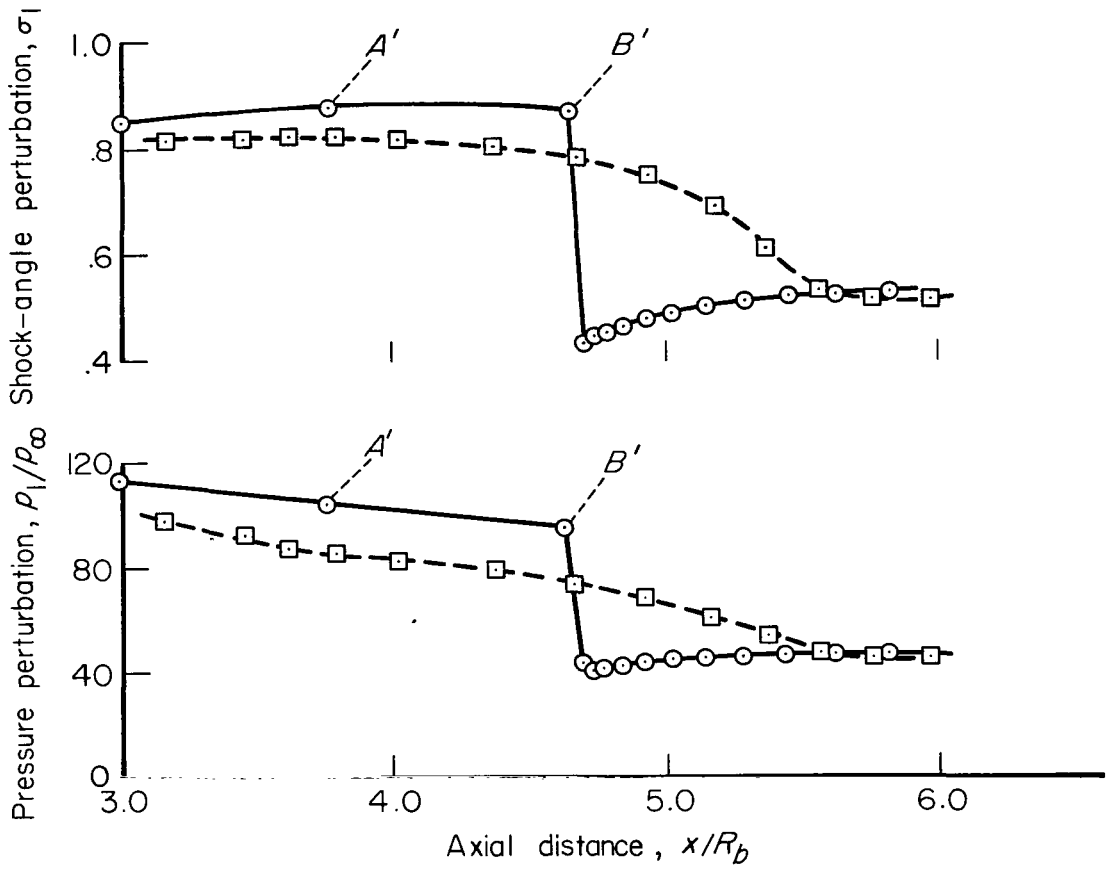

(a) Shock.

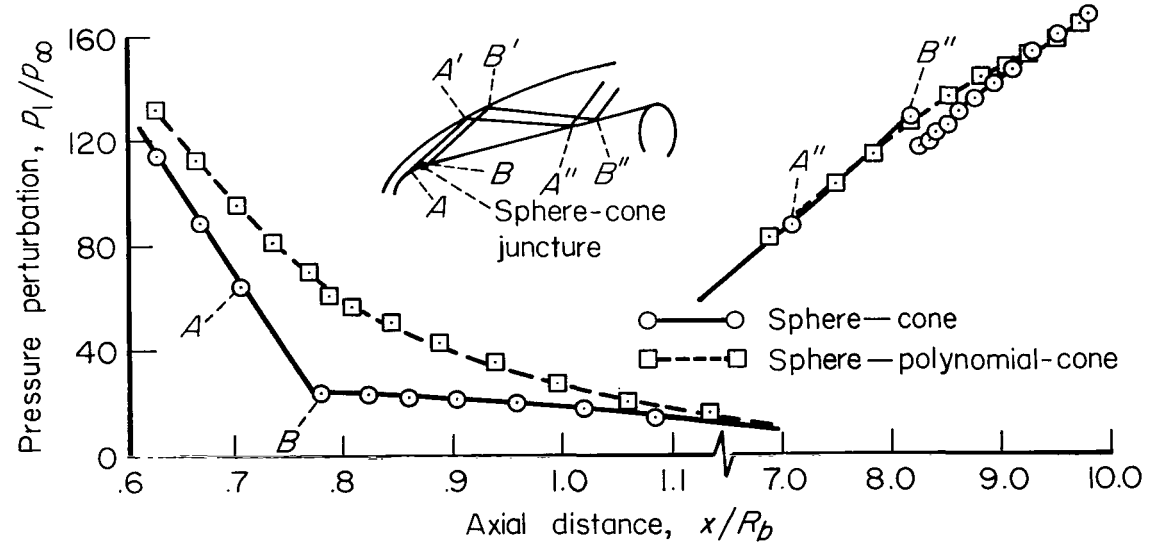

(b) Body.

Figure 10.- Effect of the transition curve between sphere and cone body segments on the discontinuous perturbation solutions.

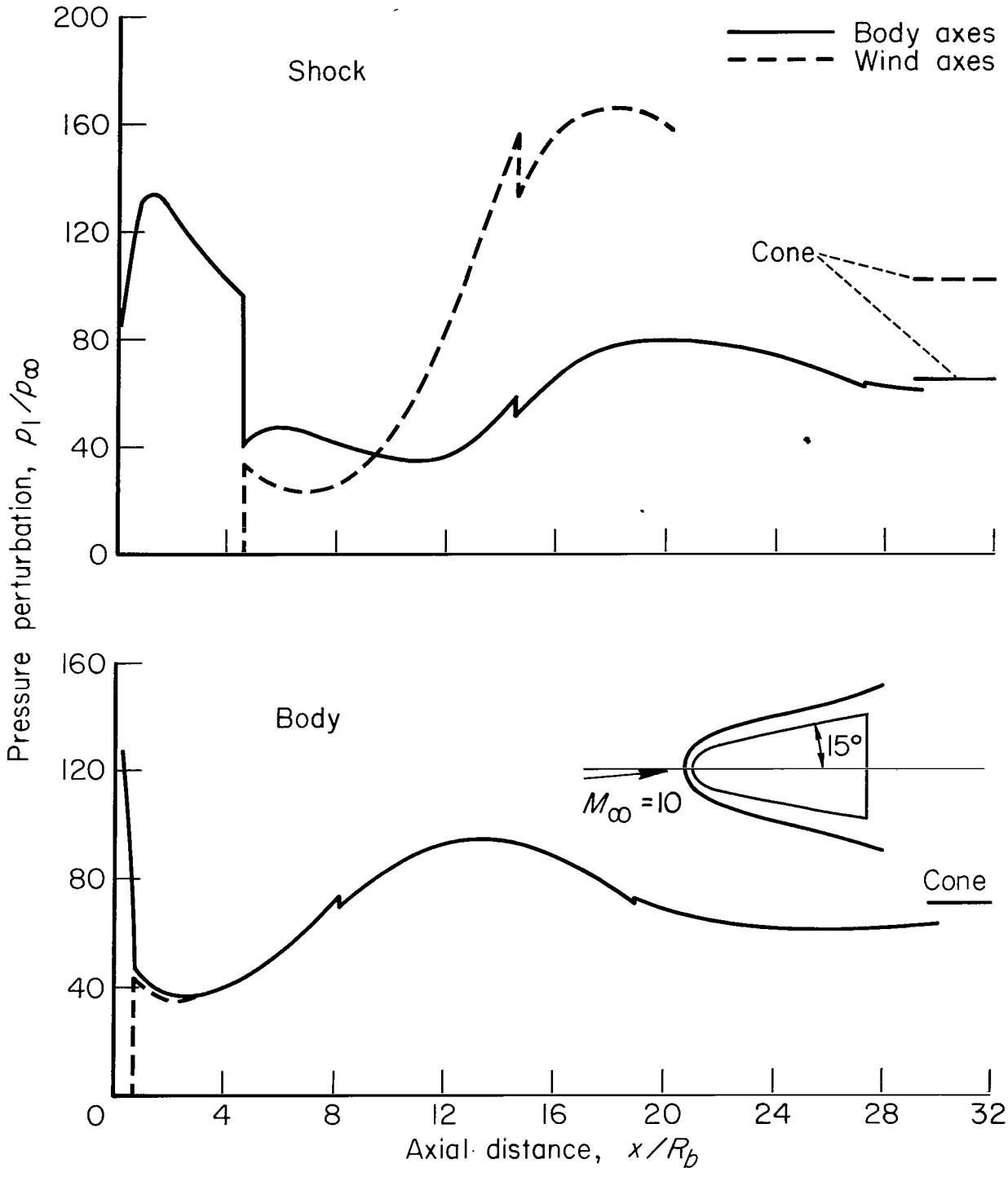

(a) Pressure perturbation.

Figure 11.- Comparison of first-order perturbation variables in terms of wind and body axes for a spherically blunted 15° cone; M_∞ = 10.

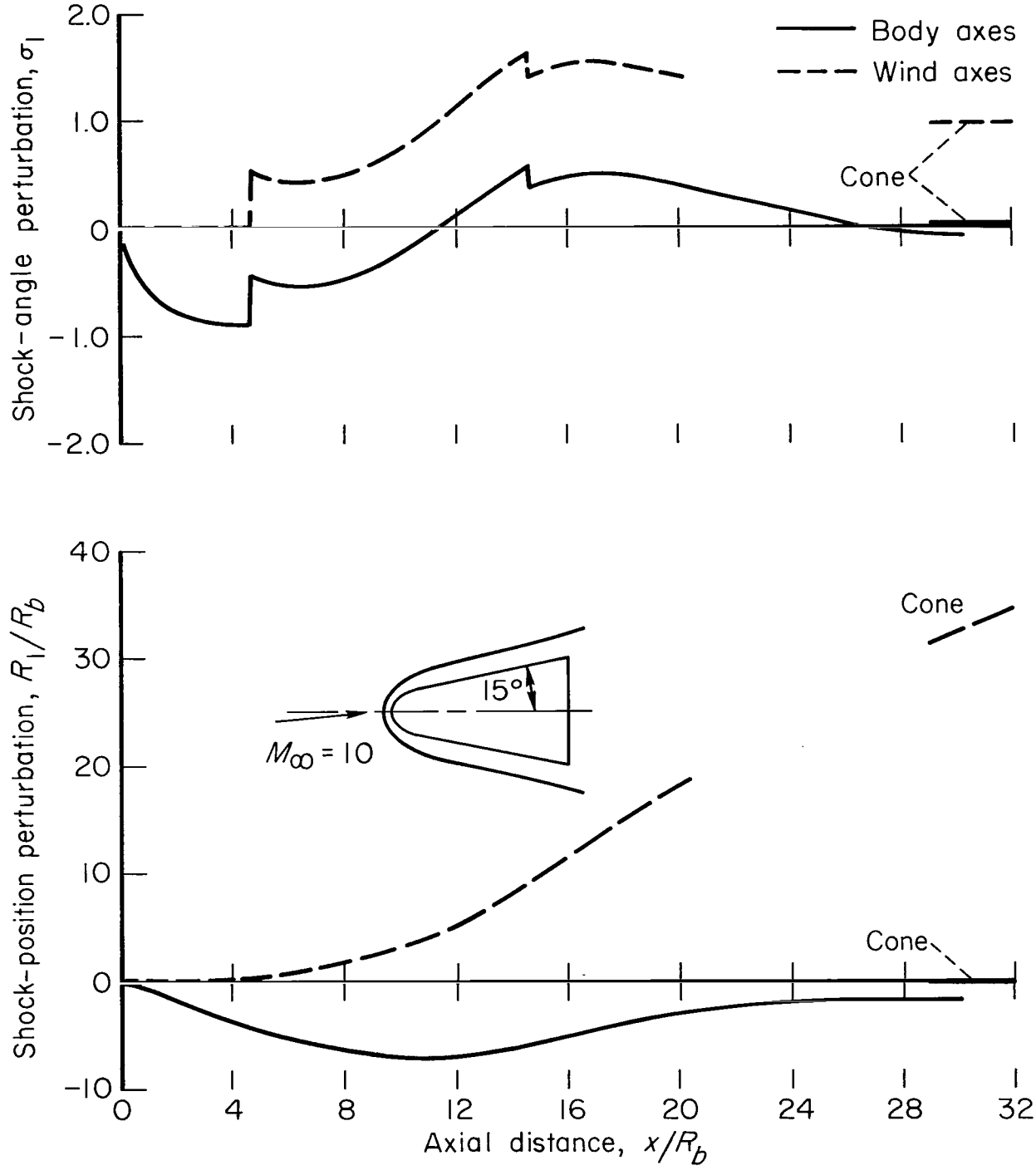

(b) Shock position and angular perturbations.

Figure 11.- Concluded.

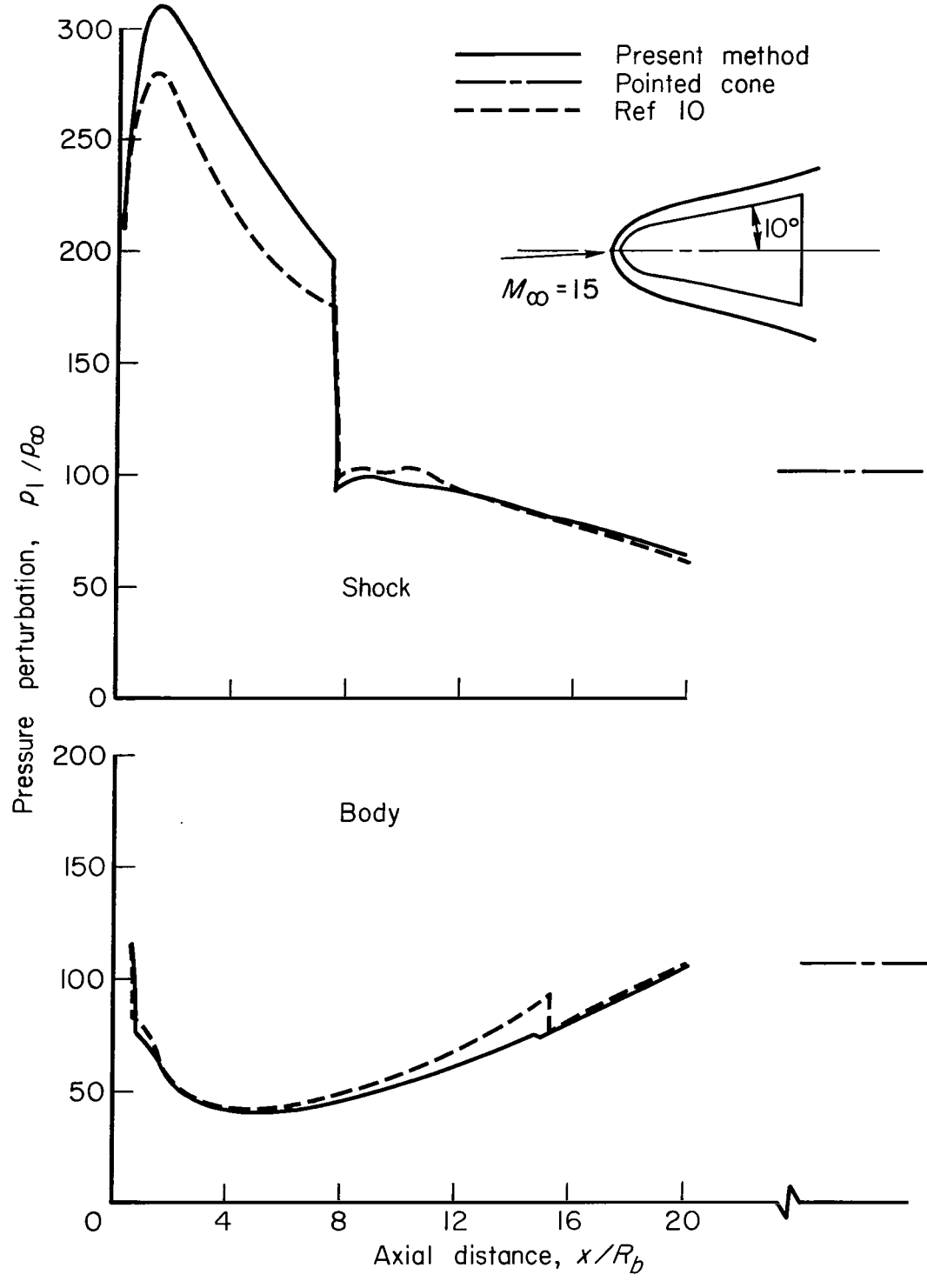

(a) Pressure perturbation.

Figure 12.- Axial variation of first-order perturbation variables for a spherically blunted 10° cone; $M_\infty = 15$ (body axes).

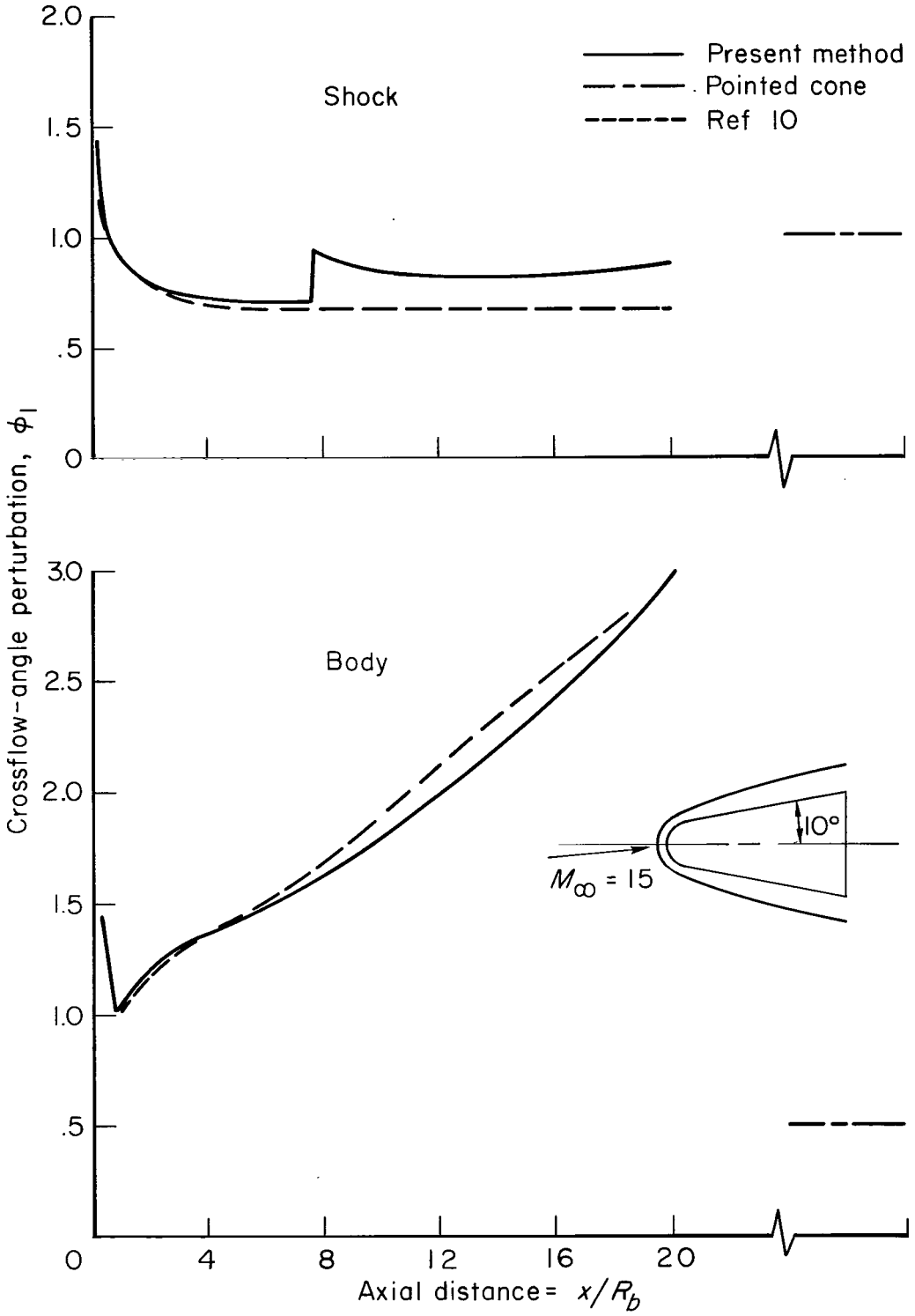

(b) Crossflow angle.

Figure 12.- Continued.

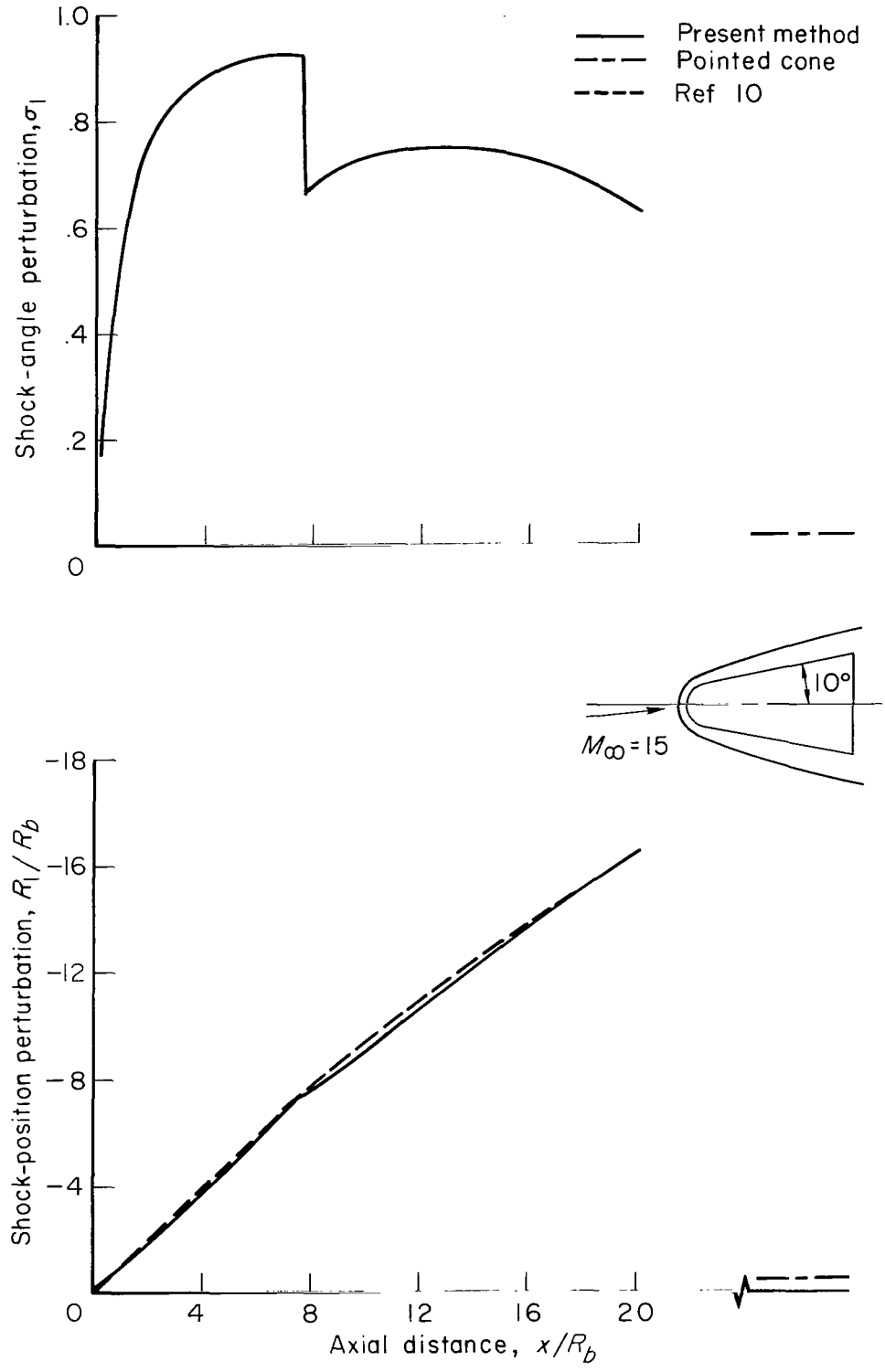

(c) Shock position and angular perturbations.

Figure 12.- Concluded.

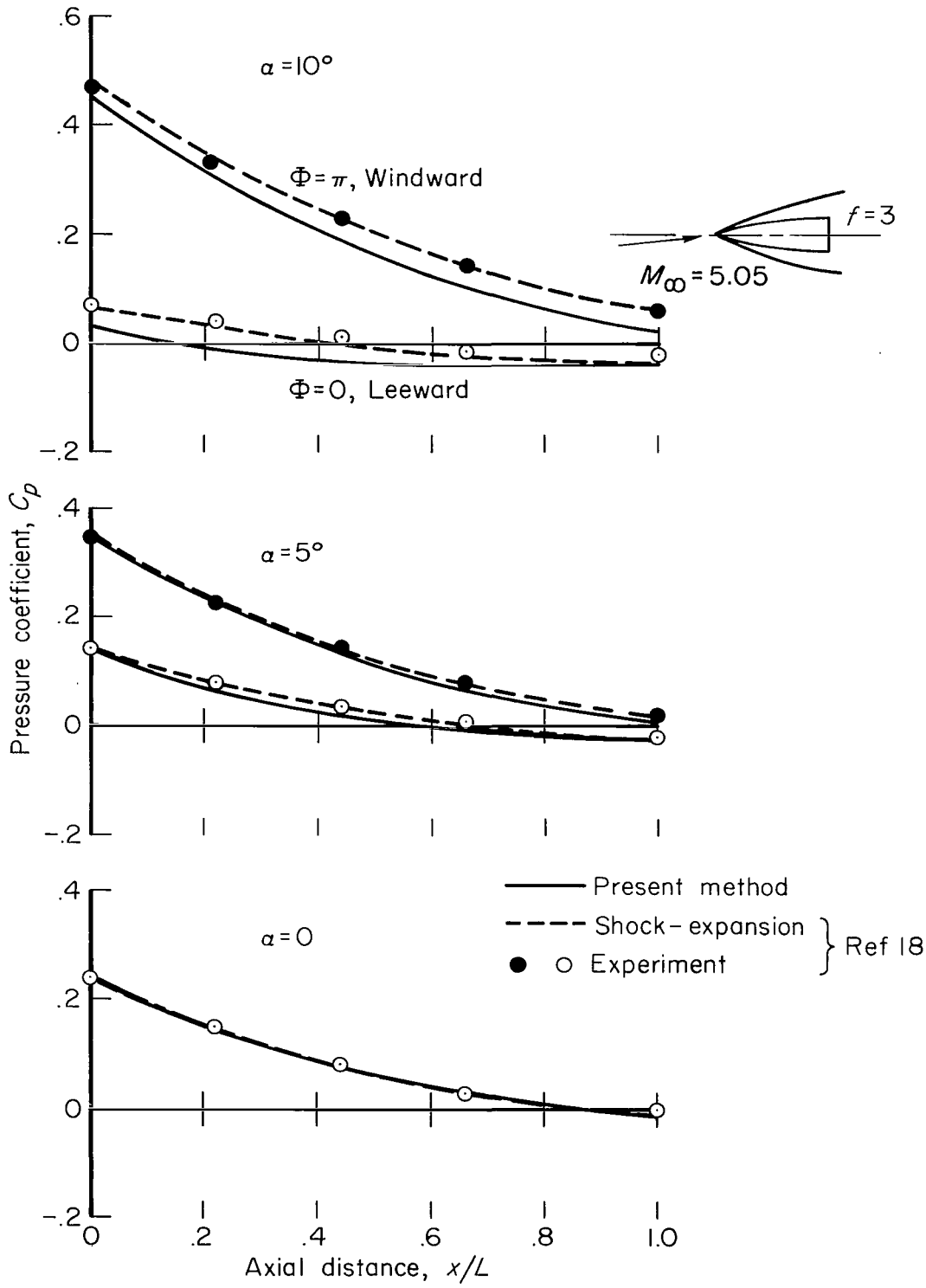

Figure 13.- Surface pressure coefficients for an ogive of fineness ratio 3; $M_\infty = 5.05$.

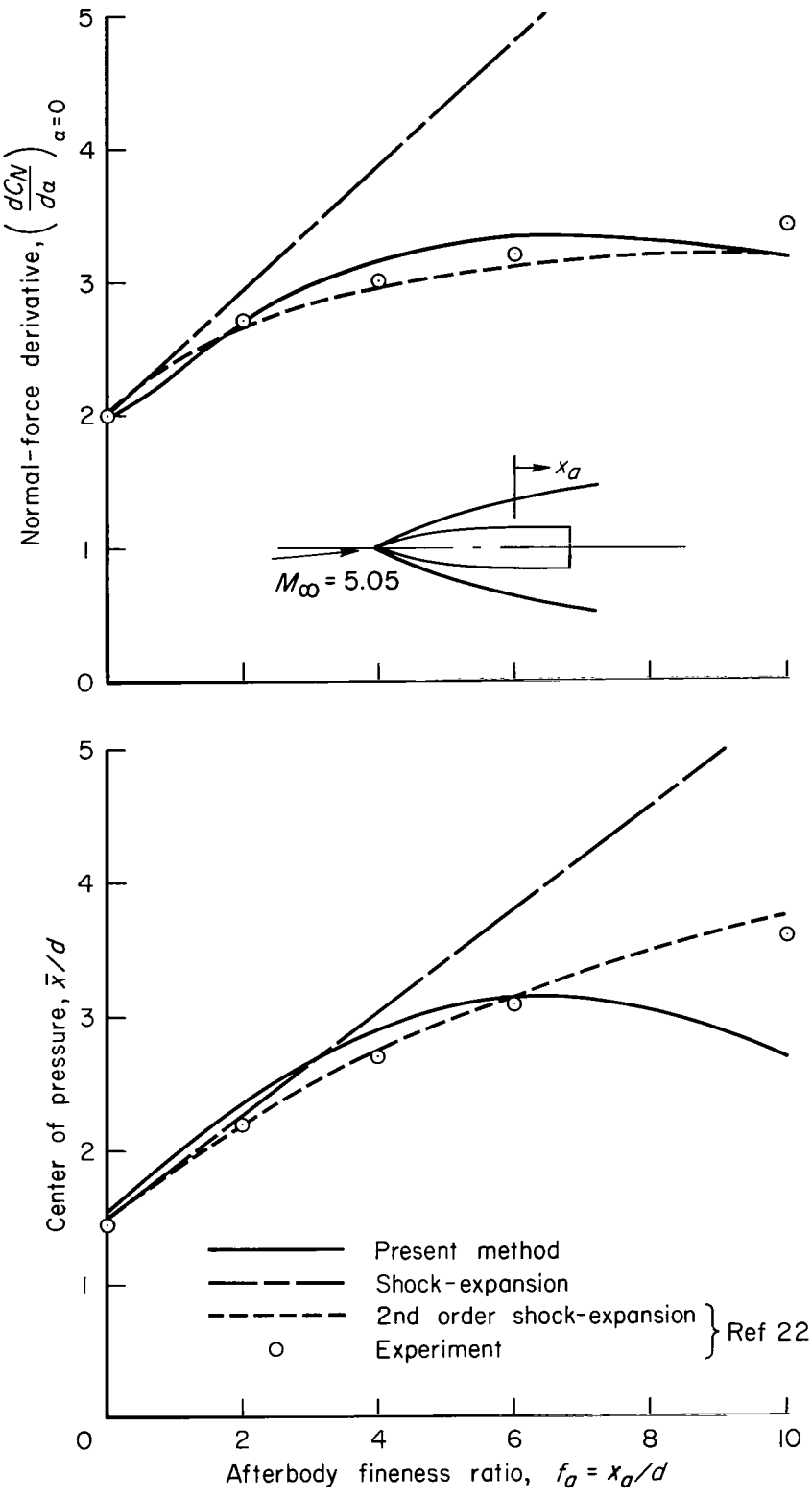

Figure 14.- Normal-force derivative and center of pressure for an ogive of fineness ratio 3 with a cylindrical afterbody; $M_\infty = 5.05$.

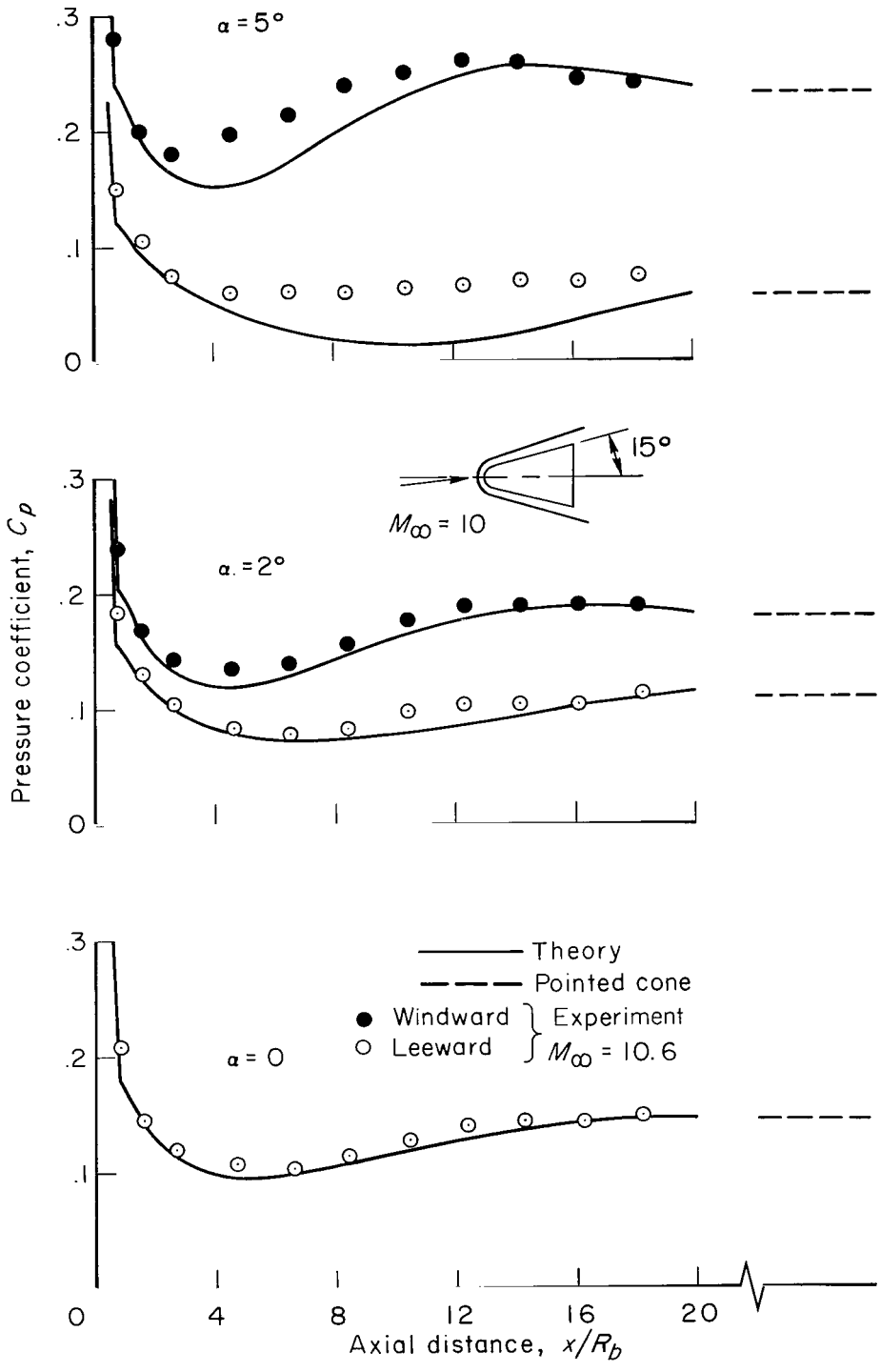

(a) Sphericallly blunted 15° cone.

Figure 15.- Surface pressure coefficients for yawed sphere cones.

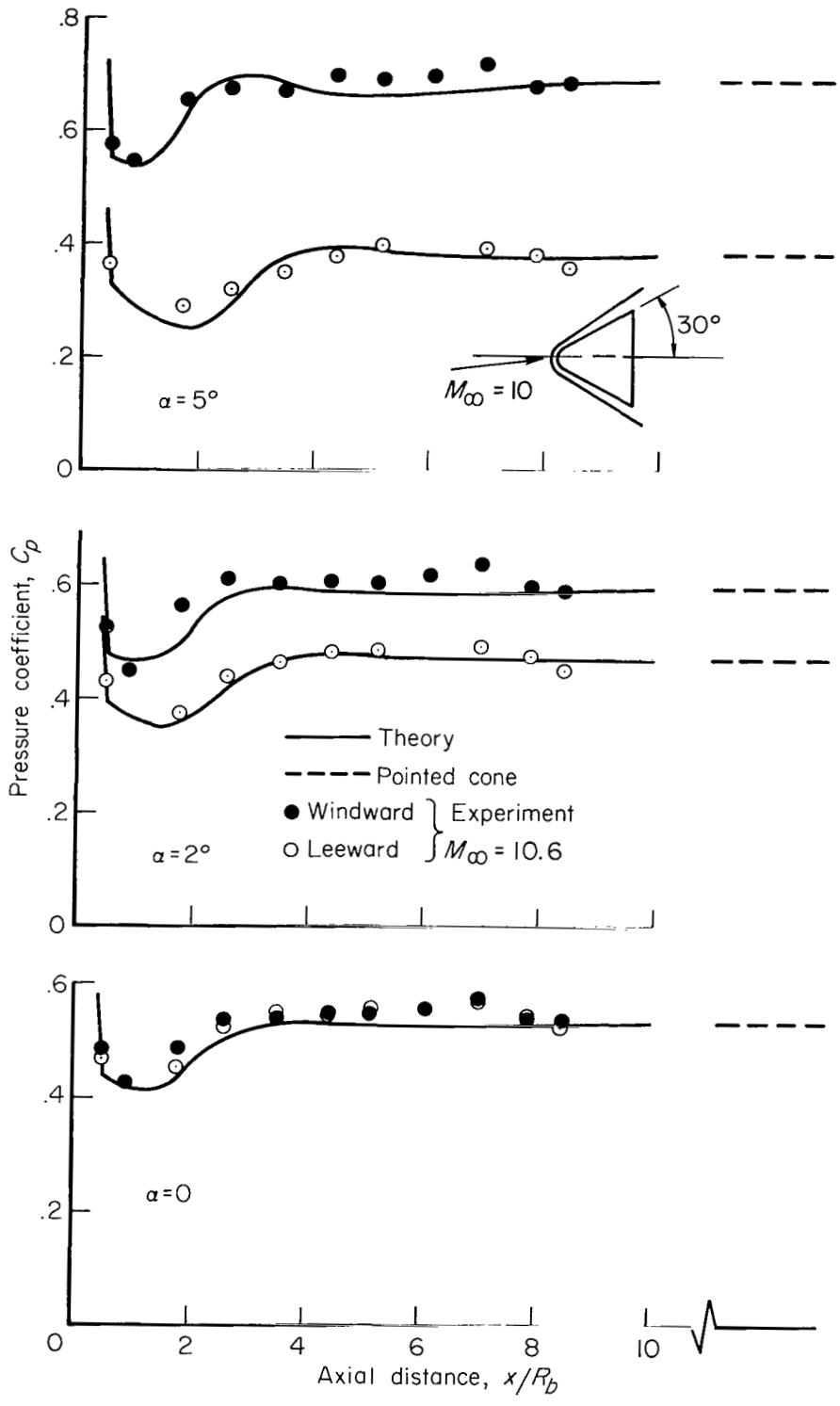

(b) Spherically blunted 30° cone.

Figure 15.- Concluded.

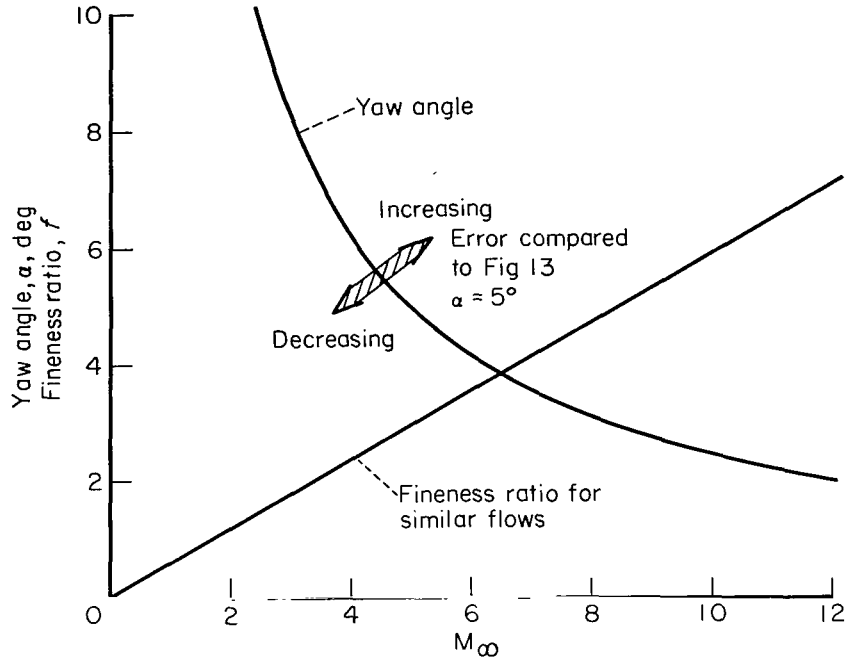

(a) Effect of Mach number.

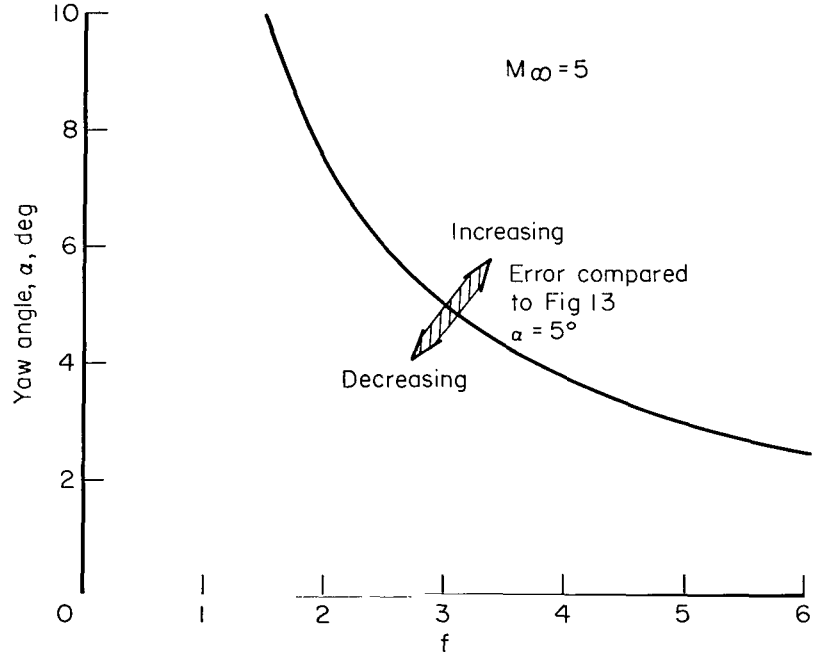

(b) Effect of fineness ratio for fixed Mach number.

Figure 16.- Variation of yaw angle for similar hypersonic flows; $K_T = M_\infty/f = 5/3$, $K_\alpha = M_\infty \alpha = 25$.

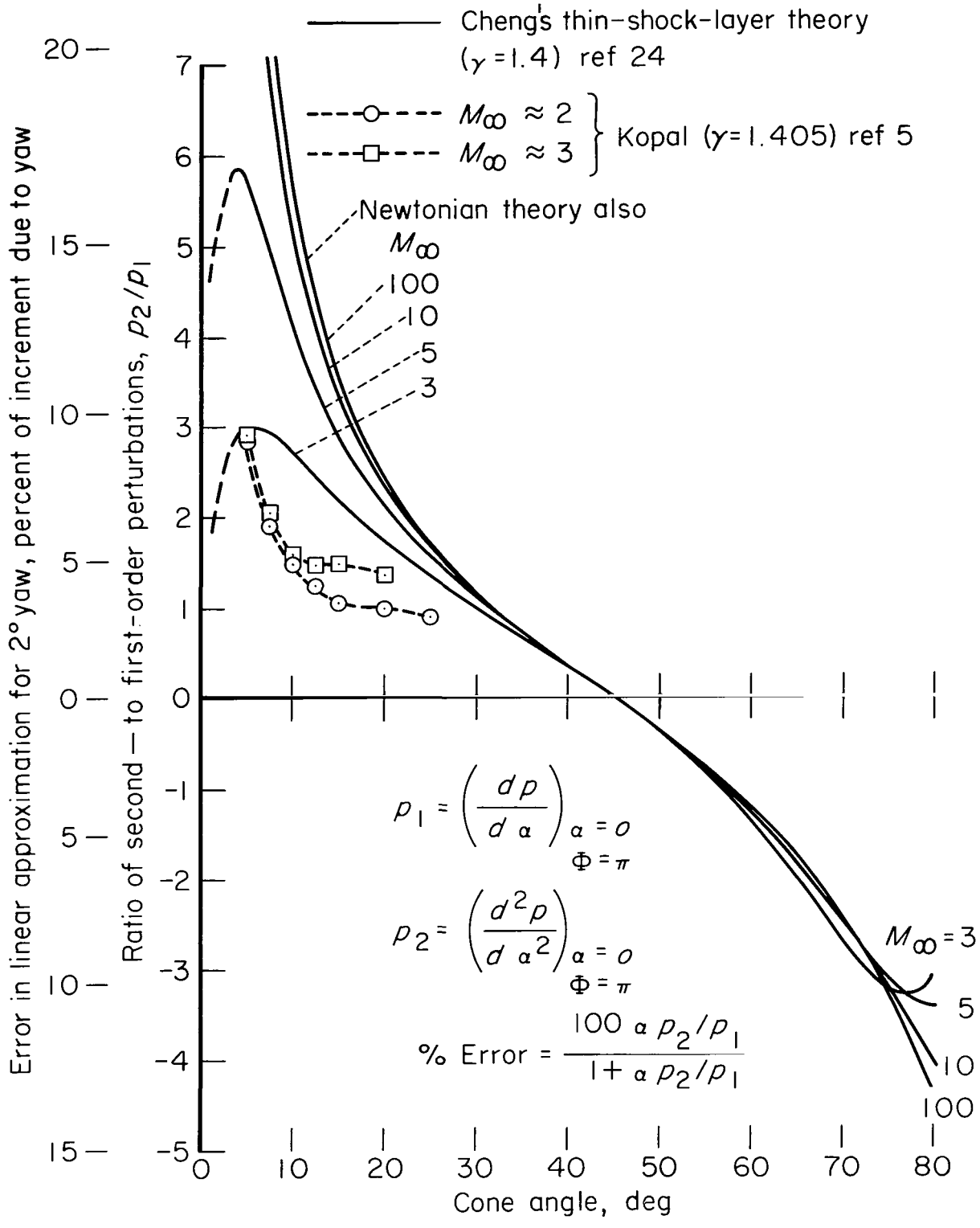

Figure 17.- Estimated error in the linear approximation to the surface pressure on cones (third and higher order terms neglected).

"The aeronautical and space activities of the United States shall be conducted so as to contribute . . . to the expansion of human knowledge of phenomena in the atmosphere and space. The Administration shall provide for the widest practicable and appropriate dissemination of information concerning its activities and the results thereof."

—NATIONAL AERONAUTICS AND SPACE ACT OF 1958

NASA SCIENTIFIC AND TECHNICAL PUBLICATIONS

TECHNICAL REPORTS: Scientific and technical information considered important, complete, and a lasting contribution to existing knowledge.

TECHNICAL NOTES: Information less broad in scope but nevertheless of importance as a contribution to existing knowledge.

TECHNICAL MEMORANDUMS: Information receiving limited distribution because of preliminary data, security classification, or other reasons.

CONTRACTOR REPORTS: Technical information generated in connection with a NASA contract or grant and released under NASA auspices.

TECHNICAL TRANSLATIONS: Information published in a foreign language considered to merit NASA distribution in English.

TECHNICAL REPRINTS: Information derived from NASA activities and initially published in the form of journal articles.

SPECIAL PUBLICATIONS: Information derived from or of value to NASA activities but not necessarily reporting the results of individual NASA-programmed scientific efforts. Publications include conference proceedings, monographs, data compilations, handbooks, sourcebooks, and special bibliographies.

Details on the availability of these publications may be obtained from:

SCIENTIFIC AND TECHNICAL INFORMATION DIVISION

NATIONAL AERONAUTICS AND SPACE ADMINISTRATION

Washington, D.C. 20546